iScience

CellPress

Article

High-Energy-Level Blue Phosphor for Solution-Processed White Organic Light-Emitting Diodes with Efficiency Comparable to Fluorescent Tubes

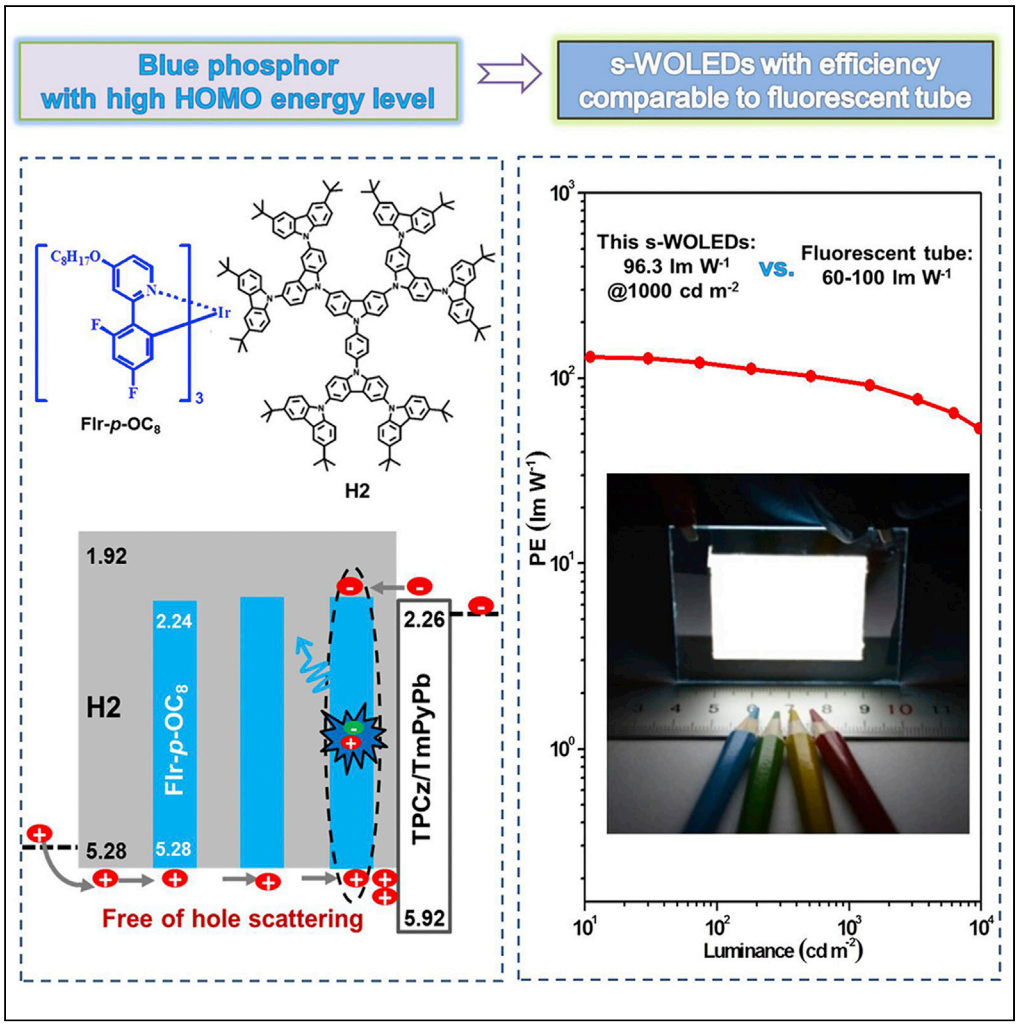

Shumeng Wang, Lei Zhao, Baohua Zhang, Junqiao Ding, Zhiyuan Xie, Lixiang Wang, Wai-Yeung Wong

bhzhang512@ciac.ac.cn (B.Z.)
junqiaod@ciac.ac.cn (J.D.)
wai-yeung.wong@polyu.edu.hk (W.-Y.W.)

HIGHLIGHTS

High-energy-level blue phosphor FIr-*p*-OC_8 is developed by alkoxyl substitution

Matched HOMO levels between dendritic host and blue-emitting dopant

Free of hole scattering to promote direct exciton formation on blue phosphor

Record-high power efficiency of 96.3 lm W^{-1} at 1,000 cd m^{-2} for solution-processed WOLEDs

Wang et al., iScience 6, 128–137
August 31, 2018
https://doi.org/10.1016/j.isci.2018.07.016

iScience

CellPress

Article

High-Energy-Level Blue Phosphor for Solution-Processed White Organic Light-Emitting Diodes with Efficiency Comparable to Fluorescent Tubes

Shumeng Wang,[1] Lei Zhao,[1] Baohua Zhang,[1,*] Junqiao Ding,[1,2,5,*] Zhiyuan Xie,[1,2] Lixiang Wang,[1,2] and Wai-Yeung Wong[3,4,*]

SUMMARY

A high-energy-level blue phosphor FIr-*p*-OC_8 has been developed for solution-processed white organic light-emitting diodes (WOLEDs) with comparable fluorescent tube efficiency. Benefiting from the electron-donating nature of the introduced alkoxy, FIr-*p*-OC_8 shows not only efficient blue light but also elevated highest occupied molecular orbital/lowest unoccupied molecular orbital levels to well match the dendritic host H2. Consequently, the hole scattering between FIr-*p*-OC_8 and H2 can be prevented to favor the direct exciton formation on the blue phosphor, leading to reduced driving voltage and thus improved power efficiency. By exploiting this approach, a maximum power efficiency of 68.5 lm W^{-1} is achieved for FIr-*p*-OC_8-based white devices, slightly declining to 47.0 lm W^{-1} at a practical luminance of 1,000 cd m^{-2}. This efficiency can be further raised to 96.3 lm W^{-1} @ 1,000 cd m^{-2} when a half-sphere is applied to increase light out-coupling. We believe that our results can compete with commercial fluorescent tubes, representing an important progress in solution-processed WOLEDs.

INTRODUCTION

White organic light-emitting diodes (WOLEDs) have attracted intense academic and industrial attention owing to their potential to replace fluorescent tubes for applications in energy-saving lightings (Kido et al., 1995; Sun et al., 2006; Reineke et al., 2009; Park et al., 2008; Su et al., 2008; Wang et al., 2009; Kamtekar et al., 2010; Chang et al., 2013; Ou et al., 2014; Ding et al., 2015; Zhou et al., 2015; Liu et al., 2016; Wu et al., 2008, 2009, 2016; Huang et al., 2009; Zou et al., 2011; Fu et al., 2012; Zhang et al., 2012, 2013; Aizawa et al., 2014; Chiba et al., 2015). Nowadays most of the attention is focused on vacuum-deposited WOLEDs (v-WOLEDs) (Ou et al., 2014; Ding et al., 2015; Zhou et al., 2015; Liu et al., 2016; Wu et al., 2016). Since the first report in 1995 (Kido et al., 1995), the power efficiency (PE) of v-WOLEDs has been significantly improved and has surpassed those of the commercial fluorescent tubes (60–100 lm W^{-1}, the threshold for practical applications) (Reineke et al., 2009; Ou et al., 2014; Ding et al., 2015). Nevertheless, solution-processed WOLEDs (s-WOLEDs) are under less investigation, although they are believed to be superior to v-WOLEDs in view of the advantages including low cost, large area, and flexible device fabrication (Wu et al., 2008, 2009; Huang et al., 2009; Zou et al., 2011; Fu et al., 2012; Zhang et al., 2012, 2013; Aizawa et al., 2014; Chiba et al., 2015). Their PE remains far away from the fluorescent tube efficiency even if transition-metal-containing phosphors are used to harvest both singlet and triplet excitons to increase the external quantum efficiency (EQE) (Wu et al., 2008, 2009; Zou et al., 2011; Fu et al., 2012; Zhang et al., 2012, 2013; Aizawa et al., 2014; Chiba et al., 2015). Therefore, the accompanying high driving voltage may account for the poor PE of s-WOLEDs because it is directly proportional to the ratio of EQE to driving voltage (PE $\propto$ EQE/V).

A single emitting layer (EML) device structure (Wu et al., 2008, 2009; Huang et al., 2009; Zou et al., 2011; Fu et al., 2012; Zhang et al., 2012, 2013; Aizawa et al., 2014), which consists of a host doped with blue and long-wavelength phosphor, is usually adopted in s-WOLEDs since the layer beneath could be dissolved by the solution deposition of a subsequent layer. Considering the negligible contribution from the long-wavelength phosphor with an extremely low doping concentration in EML, the host and blue phosphor are two critical factors that are related to the high driving voltage originating from the limited charge injection and transport. First, a suitable host with a triplet energy higher than that of blue phosphor is desirable to avoid triplet exciton back transfer from the dopant to the host (Ding et al., 2009; Lee and Lee, 2013; Park et al., 2013; Lee et al., 2015; Seino et al., 2014). So an increased driving voltage should be provided to overcome large energy barriers before carriers (holes and/or electrons) are injected into such

[1]State Key Laboratory of Polymer Physics and Chemistry, Changchun Institute of Applied Chemistry, Chinese Academy of Sciences, Changchun 130022, PRC

[2]University of Science and Technology of China, Hefei 230026, PRC

[3]Department of Applied Biology and Chemical Technology, The Hong Kong Polytechnic University, Hung Hom, Hong Kong, PRC

[4]Institute of Molecular Functional Materials and Department of Chemistry, Hong Kong Baptist University, Waterloo Road, Hong Kong, PRC

[5]Lead Contact

*Correspondence: bhzhang512@ciac.ac.cn (B.Z.), junqiaod@ciac.ac.cn (J.D.), wai-yeung.wong@polyu.edu.hk (W.-Y.W.)

https://doi.org/10.1016/j.isci.2018.07.016

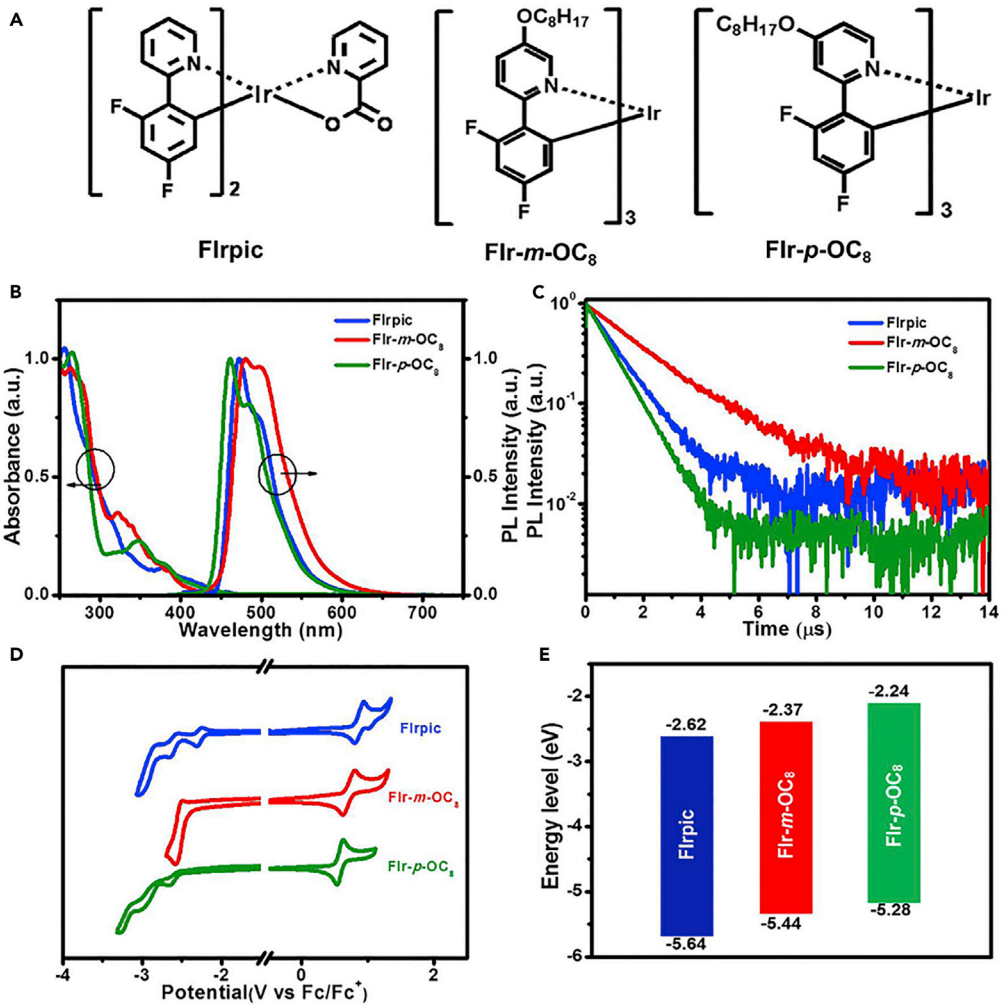

Figure 1. Design of High-Energy-Level Blue Phosphors

(A) Molecular structures of blue phosphors (FIrpic, FIr-*m*-OC_8 and FIr-*p*-OC_8).

(B) UV-Vis absorption spectra in dichloromethane (DCM) together with photoluminescent (PL) spectra in toluene (The black circles and arrows indicate the corrsponding vertical axis for each data curves).

(C) PL decay curves in toluene.

(D) Cyclic voltammograms in solution using 0.1M n-Bu_4NClO_4 as supporting electrolyte at a scan rate of 100 mV s^{-1}.

(E) HOMO/LUMO level alignment of the blue phosphors.

Also see Scheme S1 and Figure S1.

wide-band-gap host. Second, either the highest occupied molecular orbital (HOMO) level or the lowest unoccupied molecular orbital (LUMO) level of the blue phosphor does not match with those of the host used. The resultant charge trapping or scattering may bring about the enhancement of driving voltage by decreasing the charge transport of the EML (Tsung and So, 2008;Li et al., 2011, 2012a, 2012b, 2014; Schmechel and von Seggern, 2004; Tong et al., 2007; von Malm et al., 2001).

Aiming at low-voltage-driving and thus power-efficient s-WOLEDs, the first challenge is to develop solution-processible host materials that exhibit appropriate energy levels to ensure efficient charge injection without sacrificing high triplet energy. Recently, a dendritic oligocarbazole molecule H2 has been demonstrated as a good host for the blue phosphor iridium(III)[bis(4,6-difluorophenyl)-pyridinato-N,C2]-picolinate (FIrpic) (Ding et al., 2009). When compared with the archetypical high-triplet-energy polymeric host poly(N-vinylcarbazole) (PVK) with a deep HOMO level of −5.9 eV, H2 possesses a triplet energy as high as 2.9 eV and an elevated HOMO level up to −5.28 eV simultaneously. As a result of the reduced hole injection barrier from PVK to H2, the PE of H2-based blue device is improved from 8.3 to 15.4 lm W^{-1}.

Material	λ_{abs}(logε)[a] (nm)	λ_{em}[b] (nm)	PLQY[c]	τ(μs)[d]	E_{ox}[e] (V)	E_{red}[e] (V)	HOMO[f] (eV)	LUMO (eV)	T_1[h] (eV)	T_m/T_d (°C)
H2	242 (5.5), 268 (5.1), 288 (5.1), 298 (5.2), 350 (4.5)	391, 408	–	–	0.48	–	−5.28	−1.91[g]	2.86	–/–
FIrpic	256 (4.7), 381 (3.8), 412 (3.5), 427 (3.3), 456 (2.8)	472, 499	0.60	1.02	0.84	−2.18	−5.64	−2.62[f]	2.63	ND/330
FIr-*m*-OC_8	244 (4.7), 263 (4.6), 323 (4.2), 371 (3.8), 379 (3.7)	481, 497	0.23	1.96	0.64	−2.43	−5.44	−2.37[f]	2.58	155/337
FIr-*p*-OC_8	265 (4.8), 347 (4.1), 381 (3.9), 417 (3.4), 448 (2.9)	462, 485	0.78	0.85	0.48	−2.56	−5.28	−2.24[f]	2.69	222/341

Table 1. Summary of Photophysical, Electrochemical, and Thermal Properties for the Dendritic Host and Blue Phosphors

Also see Figures S2–S4, and Table S1.

[a]Measured in DCM at 298 K with a concentration of 10^{-5} M.

[b]Measured in toluene at 298 K with a concentration of 10^{-5} M.

[c]Measured in degassed toluene at 298 K excited at 350 nm with a concentration of 10^{-5} M using a calibrated integrating sphere.

[d]Measured in degassed toluene at 298 K, and the lifetimes were obtained by a monoexponential fit of PL decay curves.

[e]E_{ox} is the first oxidation onset measured in DCM, and E_{red} is the first reduction onset measured in DMF.

[f]The HOMO and LUMO energy levels were calculated according to the equations: HOMO = -e(E_{ox}+ 4.8 V) and LUMO = -e(E_{red}+ 4.8 V).

[g]The LUMO levels are calculated according to the equation: LUMO = HOMO + E_g, where E_g is the optical bandgap estimated from the absorption onset.

[h]The triplet energy levels were calculated according to the phosphorescence peak wavelength positioned on the shortest wavelength side measured in toluene solution with a concentration of 10^{-5} M.

Further co-doping a small amount of yellow phosphor iridium(III)[5-trifluoromethyl-2-(9,9-diethylfluoren-2-yl)pyridine] (Ir(FIpy-CF_3)$_3$) into the EML leads to a promising white light (Zhang et al., 2012), showing a PE of 23.3 lm W^{-1} at a practical luminance of 1,000 cd m^{-2}. In this case, although the host is well modified to facilitate hole injection, hole transport could be obviously influenced by the associated hole scattering because the HOMO level of FIrpic (−5.64 eV) is much lower than that of H2. To solve this bottleneck, the second challenge is to design novel blue phosphors with high energy levels so as to match with those of the dendritic host. However, this important issue has rarely been addressed to date.

Here we present the realization of power-efficient s-WOLEDs with PE approaching 100 lm W^{-1} at a luminance of 1,000 cd m^{-2} by using a newly developed high-energy-level blue phosphor FIr-*p*-OC_8 (Figure 1). Unlike the commonly used FIrpic (−5.64/-2.62 eV), the para substitution of alkoxy group endows FIr-*p*-OC_8 with elevated HOMO/LUMO levels of −5.28/-2.24 eV while maintaining efficient blue emission. When combined with the dendritic host H2 (Figure 3D), the hole scattering between FIr-*p*-OC_8 and H2 can be effectively prevented because of their matched HOMO levels, thus allowing excitons to be formed directly on FIr-*p*-OC_8. With this approach, low driving voltage and high PE have been successfully achieved for the solution-processed white light-emitting device based on FIr-*p*-OC_8, revealing a state-of-art PE of 68.5 lm W^{-1} at the maximum and 47.0 lm W^{-1} at 1,000 cd m^{-2}. Also, when a half-sphere is applied to increase the light out-coupling, these efficiencies can be further raised to 130.1 and 96.3 lm W^{-1}, respectively. To our knowledge, such performance is the highest ever reported so far for s-WOLEDs, which could even compete with those of commercial fluorescent tubes.

RESULTS AND DISCUSSION

Molecular Design

To tune the energy level of blue phosphors, the alkoxy group with strong electron-donating capability is introduced into the *meta* and *para* positions to the N atom in the 2-(2′,4′-difluorophenyl)pyridine ligand, and the corresponding homoleptic Ir complexes FIr-*m*-OC_8 and FIr-*p*-OC_8 are synthesized, respectively (Figure 1A). During the procedure (Scheme S1), a convenient post-modification is adopted and begins with the preparation of an emissive Ir core functionalized with three reactive hydroxyl groups (FIr-*m*-OH

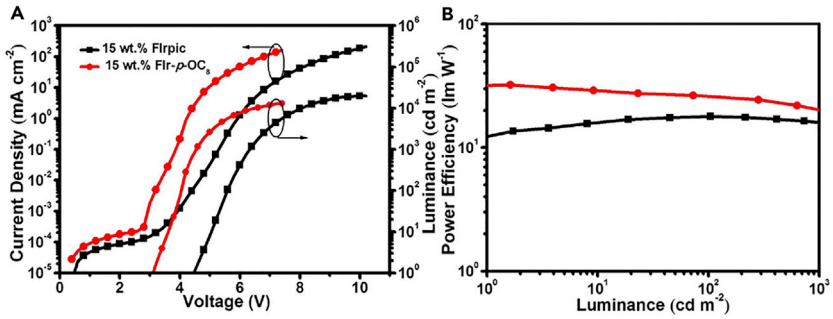

Figure 2. Performance Comparison between FIrpic- and FIr-*p*-OC_8-Based Blue Devices with the Same Doping Concentration (15 wt. %)

(A) Current density-voltage-luminance characteristics (The black circles and arrows indicate the corrsponding vertical axis for each data curves).

(B) Power efficiency-luminance characteristics.

Also see Figures S5 and S6, and Table S2.

and FIr-*p*-OH), which subsequently reacts with octyl bromide to give the final Ir complexes. Their detailed synthesis and characterization are provided in the Supplemental Information.

Figures 1B and 1C plot the steady and transient photoluminescence spectra of the complexes in toluene solution, respectively. With respect to FIrpic (λ_{em} = 472 nm), as one can see, FIr-*m*-OC_8 displays a red-shifted emission at 481 nm, whereas a hypsochromic shift (λ_{em} = 462 nm) is observed for FIr-*p*-OC_8 (Table 1). In addition, the exited state lifetime in toluene solution of FIr-*p*-OC_8 (0.85 μs) is found to be shorter than those of FIrpic (1.02 μs) and FIr-*m*-OC_8 (1.96 μs), in good agreement with the higher photoluminescence quantum yield (PLQY) in toluene solution of FIr-*p*-OC_8 (0.78) than those of FIrpic (0.60) and FIr-*m*-OC_8 (0.23). Most importantly, as estimated from their cyclic voltammetry curves (Figure 1D), the HOMO/LUMO levels are gradually increased from −5.64/-2.62 eV of FIrpic to −5.44/-2.37 eV of FIr-*m*-OC_8 and −5.28/-2.24 eV of FIr-*p*-OC_8 (Figure 1E). The upshift of HOMO/LUMO is in good agreement with the theoretical calculations (Figure S1), indicating that the position and electron-donating effect of the alkoxy substituent can be employed to finely tailor the photophysical and electrochemical properties of blue phosphors.

Superiority of High-Energy-Level Blue Phosphor

In view of the obtained high-lying HOMO/LUMO levels, blue-shifted emission, high Φ_{PL}, and shorter lifetime, FIr-*p*-OC_8 is anticipated to be a better blue phosphor than FIrpic. To demonstrate this point, two types of monochromic devices are prepared at the same time for comparison: ITO(indium tin oxide)/PEDOT:PSS(poly(ethylenedioxythiophene):poly(styrenesulfonate))/H2:FIrpic/TPCz/TmPyPb/LiF/Al (denoted as device A) and ITO/PEDOT:PSS/H2:FIr-*p*-OC_8/TPCz/TmPyPb/LiF/Al (denoted as device B) (Figure S5). When the doping concentration grows up from 1 wt.% to 15 wt.%, the turn-on voltage for device A is monotonically increased from 3.9 to 4.5 V along with the reduced current density at the same driving voltage (Figure S6 and Table S2). On the contrary, the turn-on voltage for device B is in the range of 3.1–3.3 V, and the current density-voltage (*J-V*) characteristics remain nearly unchanged, irrespective of the doping concentration. Accordingly, device B exhibits reduced driving voltage and improved PE than device A. As depicted in Figure 2, both the *J-V* and luminance-voltage (*L-V*) curves at a 15 wt.% content shift by about 1.5 V toward a negative voltage on going from FIrpic to FIr-*p*-OC_8. Under a luminance of 100 and 1,000 cd m^{-2}, the driving voltages are significantly decreased from 5.6 to 6.3 V to 4.0 and 4.5 V. Meanwhile, the PEs are raised from 17.8 and 16.0 lm W^{-1} to 26.2 and 20.3 lm W^{-1}.

Given the same configuration, the observed difference of the device performance between FIrpic and FIr-*p*-OC_8 can be reasonably ascribed to their different energy alignments with regard to H2. In device A, holes are injected and transported in H2 but not in FIrpic since FIrpic has a deeper HOMO level than H2 (Figure 3A). On one hand, FIrpic can act as hole scatters and cause an increase of the total transit path and thus the decrease of the hole mobility. As verified by the hole-only devices (Figure 3B), the hole current at the same driving voltage is greatly lowered with increasing content of FIrpic. On the other hand, electrons can be injected from TPCz/TmPyPb either into FIrpic preferentially or into H2 through electrostatic attraction and then trapped by FIrpic as a result of the lower lying LUMO of FIrpic relative to H2. These captured electrons on FIrpic can neither escape from FIrpic due

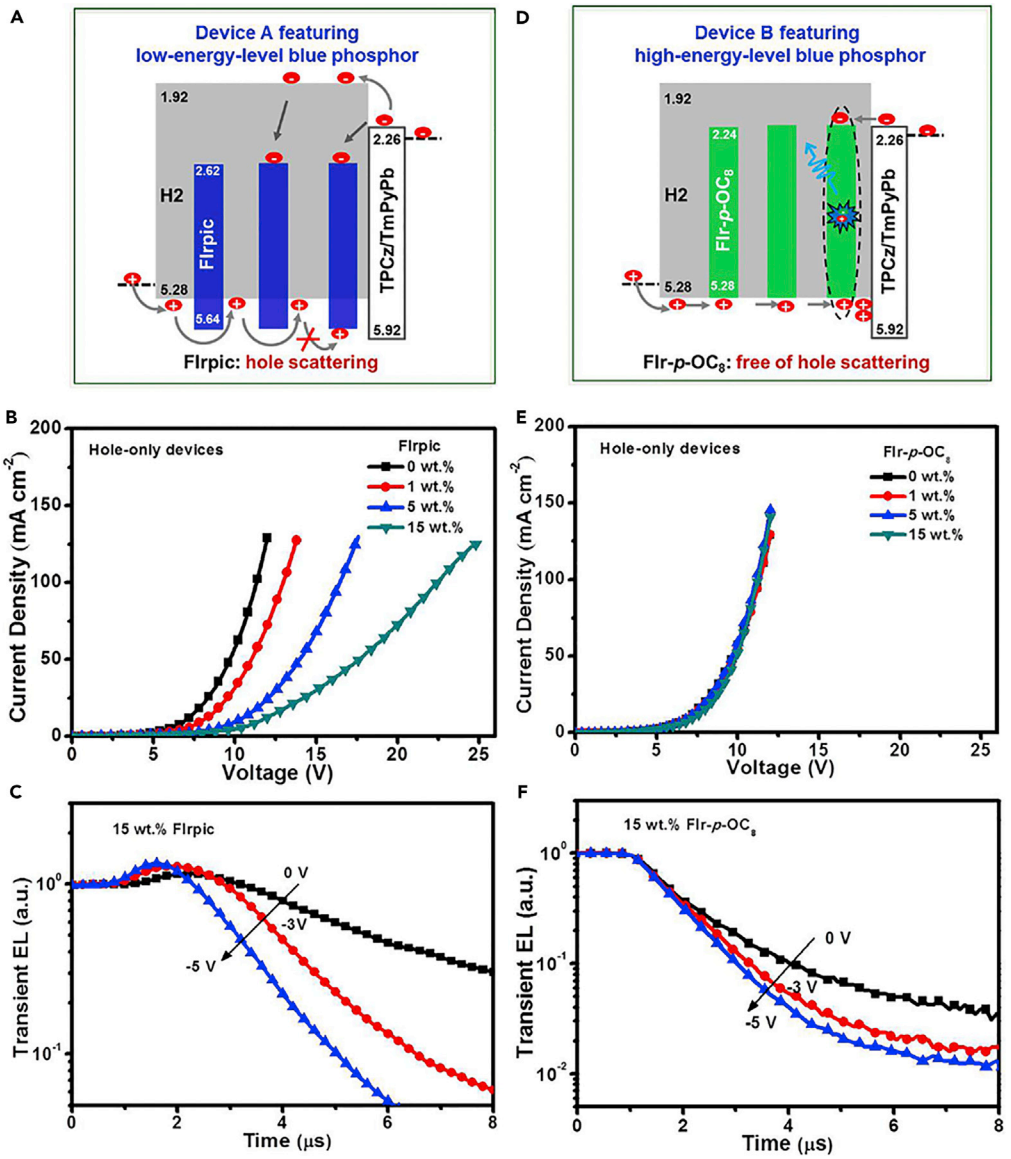

Figure 3. Analysis of the Hole Scattering-Induced Influence

(A) Working mechanism of FIrpic-based blue device.

(B) Current density-voltage characteristics of FIrpic-based hole-only devices with different doping concentration of 0, 1, 5, and 15 wt.%.

(C) Transient EL decay curves for FIrpic-based blue device with a doping concentration of 15 wt. %.

(D) Working mechanism of FIr-*p*-OC_8-based blue device.

(E) Current density-voltage characteristics of FIr-*p*-OC_8-based hole-only devices with different doping concentration of 0, 1, 5, and 15 wt.%.

(F) Transient EL decay curves for FIr-*p*-OC_8-based blue device with a doping concentration of 15 wt.%.

Also see Figure S4 and Table S1.

to the large electron-trapping depth between FIrpic and H2 (0.70 eV) nor form the radiative excitons because holes occur scarcely in FIrpic due to the existing hole scattering. Consequently, electrons would be inevitably stored on FIrpic molecules to some extent, which is further confirmed by time-resolved electroluminescence measurements (Liu et al., 2011; Weichsel et al., 2012). As one can see in Figure 3C, a distinct transient overshoot, corresponding to an electron storage, is distinctly observed for device A after voltage turn-off. When a negative postpulse bias is applied from 0 to −3 and −5 V, the overshoot time is gradually shortened, associated with the enhanced overshoot intensity. In other words, the existence of hole scattering in device A would cause both

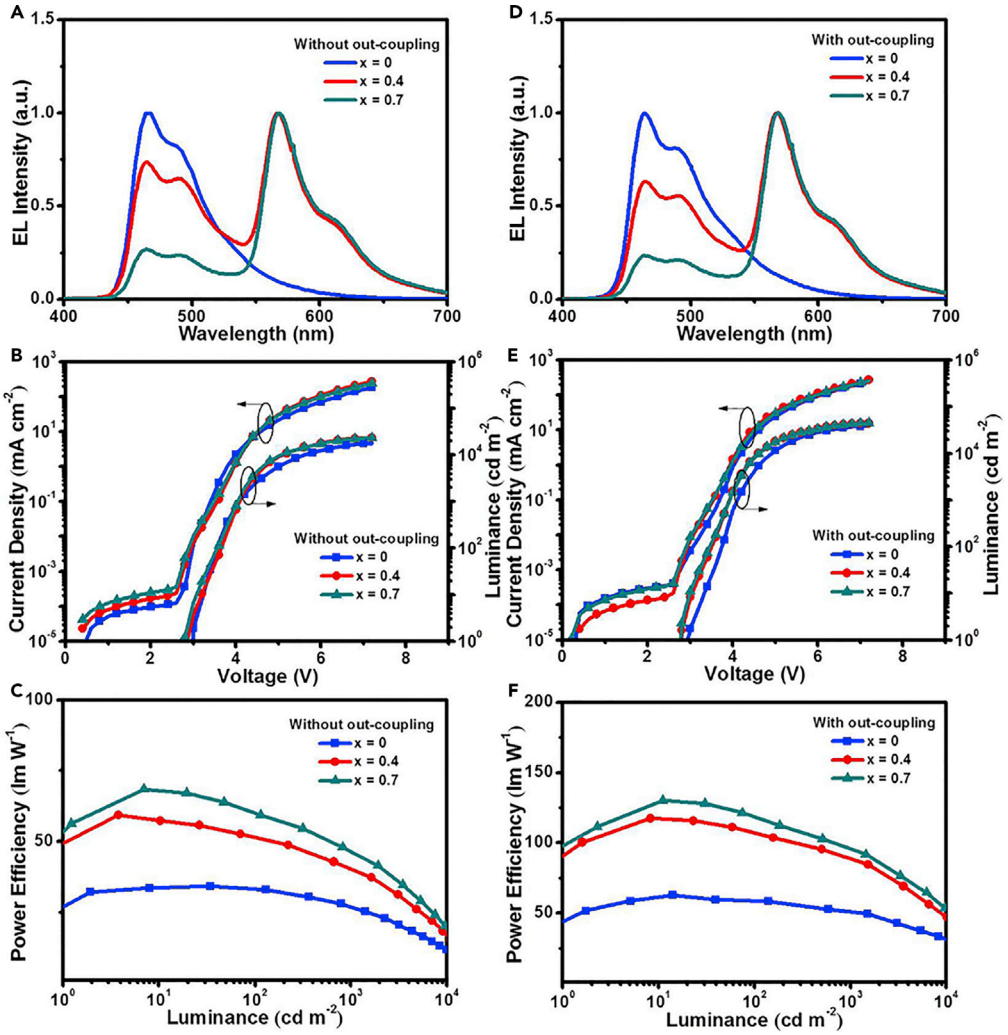

Figure 4. Performance of FIr-*p*-OC_8-Based Blue and White Devices with an EML Composed of H2, 25 wt.%; FIr-*p*-OC_8, x wt.% Ir(FIpy-CF_3)$_3$

(A–C) EL spectra at 1,000 cd m^{-2}; current density-voltage-luminance characteristics; and power efficiency as a function of luminance for devices without out-coupling (The black circles and arrows indicate the corrsponding vertical axis for each data curves).

(D–F) EL spectra at 1,000 cd m^{-2}; current density-voltage-luminance characteristics; and power efficiency as a function of luminance for devices with light out-coupling (The black circles and arrows indicate the corrsponding vertical axis for each data curves).

Also see Figures S5 and S7–S15, and Tables S3 and S4.

reduced hole mobility and electron accumulation on dopant, which is responsible for the inferior device performance of FIrpic.

In contrast, hole scattering is not present anymore in device B because the HOMO level of FIr-*p*-OC_8 matches well with H2. Holes can hop freely between H2 and FIr-*p*-OC_8, and hole transport is not affected by the doped blue phosphor (Figure 3D). This is consistent with the hole-only devices (Figure 3E), where the hole current is found to be independent of the doping concentration of FIr-*p*-OC_8. Meanwhile, the electrons that are energetically injected from TPCz/TmPyPb to FIr-*p*-OC_8 owing to their close LUMO levels would not accumulate on FIr-*p*-OC_8, but recombine with the holes to generate excitons directly. As shown in Figure 3F, no transient overshoot is detected for device B, implying the vanishment of electron accumulation. Therefore, the unwanted hole scattering can be eliminated in device B to favor the direct exciton generation on the blue phosphors, leading to the reduction of driving voltage and enhancement of PE.

Content of Ir(Flpy-CF_3)$_3$	V_{on} (V)	Max Performance				Device Performance at 1000/5000 cd m^{-2}				
		L (cd m^{-2})	LE (cd A^{-1})	PE (lm W^{-1})	EQE (%)	V_d (V)	LE (cd A^{-1})	PE (lm W^{-1})	EQE (%)	CIE (x, y) at 1000 cd m^{-2}
x = 0 (Without out-coupling)	2.9	17,655	37.8	34.2	19.6	4.1/4.7	34.9/27.1	26.9/17.5	18.1/14.1	(0.15, 0.26)
x = 0 (With out-coupling)	2.9	38,580	70.9	63.0	34.2	4.1/4.6	66.9/56.2	50.9/38.6	32.2/27.0	(0.16, 0.28)
x = 0.4 wt.% (Without out-coupling)	2.9	23,392	60.4	59.4	21.8	4.1/4.6	52.7/37.7	40.2/25.8	19.6/14.5	(0.34, 0.39)
x = 0.4 wt.% (With out-coupling)	2.8	44,177	120.3	117.5	42.8	3.9/4.3	110.5/85.0	88.7/61.9	41.0/32.2	(0.36, 0.40)
x = 0.7 wt.% (Without out-coupling)	2.8	23,085	69.1	68.5	23.6	4.1/4.6	59.7/43.1	47.0/29.8	20.6/15.4	(0.43, 0.44)
x = 0.7 wt.% (With out-coupling)	2.8	44,485	131.5	130.1	44.6	3.9/4.3	119.5/95.0	96.3/69.0	40.9/33.0	(0.44, 0.44)

Table 2. Summary of Device Performance for FIr-*p*-OC_8-Based Blue and White Light-Emitting Devices with an EML Composed of H2: 25 wt.% and FIr-*p*-OC_8: x wt.% Ir(Flpy-CF_3)$_3$

Also see Figures S10 and S13, and Table S4.

Solution-Processed White Devices

Promoted by the superiority of FIr-*p*-OC_8 to FIrpic in terms of the lower driving voltage and higher PE, FIr-*p*-OC_8 is then used to fabricate power-efficient s-WOLEDs. Considering the fact that the PE of FIr-*p*-OC_8 does not reach the maximum value in the range of 1–15 wt.% (Table S2), the FIr-*p*-OC_8 content doped into H2 is tuned to optimize the monochromic device performance. It is found that the best device performance is obtained at a much higher doping concentration of 25 wt.%, giving a peak PE of 34.2 lm W^{-1} (37.8 cd A^{-1}, 19.6%) with Commission Internationale de l'Eclairage (CIE) coordinates of (0.15, 0.26) (Figures 4A and S7, Tables 2 and S3). Even at a luminance of 100 and 1,000 cd m^{-2}, the PE still remains at 33.1 and 26.9 lm W^{-1}, respectively, indicative of the gentle PE roll-off. It could be ascribed to the very low driving voltage of only about 3.6/4.1 V at a luminance of 100/1,000 cd m^{-2}. In addition, compared with a device with 15 wt. % FIr-*p*-OC_8, the driving voltage at 1,000 cd m^{-2} for a device with 25 wt. % FIr-*p*-OC_8 is decreased by about 0.4 V, and the PE is correspondingly increased by about 33%. As discussed above, the formation of excitons directly on blue phosphor is mainly responsible for the efficient blue light after the elimination of hole scattering. Thus the higher content of the blue dopant into H2 could contribute more to this pathway, and result in PE improvement.

Based on such an optimized composition (H2: 25 wt.% FIr-*p*-OC_8), subsequently, an additional yellow phosphor Ir(Flpy-CF_3)$_3$ is added into the EML for the fabrication of s-WOLEDs (Figure S5). The absolute concentration of Ir(Flpy-CF_3)$_3$ is initially adjusted to be 0.4 wt.% so as to balance the blue and yellow components for the realization of a satisfactory white emission with CIE coordinates of (0.34, 0.39) (Figure 4A), close to the standard white point, viz., (0.33, 0.33). At such a low doping concentration, Ir(Flpy-CF_3)$_3$ is considered to have no influence on the device working mechanism, which is evidenced by nearly the same J-V characteristics between monochromic and two-color white lightemitting devices (Figure 4B). Similar to the monochromic device, hole scattering between host and dopant is avoided and most of the excitons are produced directly on the blue phosphor in the white device, followed by a subsequent energy transfer to the yellow phosphor to generate the white light. As a consequence, the advantages of the monochromic device, such as the ultralow driving voltage, high PE, and small efficiency roll-off, could be inherited by the white device. For example, the driving voltage is as low as 2.9, 4.1, and 4.6 V at 1, 1,000 and 5,000 cd m^{-2}, respectively. The maximum PE is 59.4 lm W^{-1}, slightly declining to 40.2 and 25.8 lm W^{-1} at a luminance of 1,000 and 5,000 cd m^{-2}, respectively (Figure 4C). Further increasing the doping concentration of Ir(Flpy-CF_3)$_3$ up to 0.7 wt.% results in a warm white light with CIE coordinates of (0.43, 0.44). Correspondingly, the PE is enhanced to 68.5 lm W^{-1} at the maximum; 47.0 lm W^{-1} at 1,000 cd m^{-2}; and 29.8 lm W^{-1} at 5,000 cd m^{-2}. When compared with FIrpic-based white-light-emitting devices showing hole scattering (23.3 lm W^{-1} at 1,000 cd m^{-2}) (Zhang et al., 2012), the PE at high luminance is increased

Year	Reference	PE at the Maximum (lm W^{-1})	PE at 1,000 cd m^{-2} (lm W^{-1})	CIE (x, y)
s-WOLEDs				
2008	Wu et al., 2008	10.0	–	(0.30, 0.47)
2009	Huang et al., 2009	23.4	–	(0.38, 0.38)
2009	Wu et al., 2009	20.3	16.8	(0.40, 0.45)
2011	Zou et al., 2011	37.4	20.7	(0.31, 0.50)
2012	Zhang et al., 2012	–	23.3	(0.38, 0.43)
2013	Zhang et al., 2013	–	22.6	(0.35, 0.41)
2014	Aizawa et al., 2014	45	18	(0.45, 0.42)
2015	Wang et al., 2015	41.8	22.8	(0.43, 0.43)
2018	This work	59.4 (w/o) 117.5 (w/-)	40.2 88.7	(0.34, 0.39) (0.36, 0.40)
2018	This work	68.5 (w/o) 130.1 (w/-)	47 96.3	(0.43, 0.44) (0.44, 0.44)
v-WOLEDs				
2008	Su et al., 2008	–	44	(0.34, 0.40)
2009	Reineke et al., 2009	– (w/o) – (w/-)	33 124	(0.45, 0.47) (0.41, 0.49)
2011	Wang et al., 2011	40.7	37.1	(0.42, 0.44)
2013	Chang et al., 2013	–	33.8	(0.44, 0.46)
2014	Zhu et al., 2014	63.2	53.4	(0.35, 0.42)
2014	Ou et al., 2014	68.8 (w/o) 132.8 (w/-)	60.0 123.4	(0.35, 0.46) (0.35, 0.46)
2015	Ding et al., 2015	64.9	49.6	(0.35, 0.46)
2015	Zhu et al., 2015	46.6	41.3	(0.45, 0.44)
2017	Wu et al., 2017	105.0	59.5	(0.40,0.48)

Table 3. Performance Comparison of the Phosphorescent WOLEDs
w/o, without out-coupling; w/-, with out-coupling.

by about two-fold for FIr-*p*-OC_8 free of hole scattering. The improvement clearly highlights the importance of high-energy-level blue phosphors in maximizing the PE of solution-processed white-emitting devices by the elimination of hole scattering.

As for the white devices built in a standard substrate-emitting architecture, the light out-coupling efficiency is approximately 20%, and the remaining 80% of the light is trapped in organic and substrate modes. Therefore, similar to the literature report (Reineke et al., 2009), a half-sphere is pasted on the bottom of the ITO glass to unlock the trapped light as much as possible. As one can see in Figure 4D, the adoption of such an out-coupling technique has little effect on the electroluminescent (EL) spectra. The CIE coordinates slightly shift from (0.34, 0.39) and (0.43, 0.44) to (0.36, 0.40) and (0.44, 0.44) for the white devices containing 0.4 wt.% and 0.7 wt.% Ir(Flpy-CF_3)$_3$, respectively. Moreover, the luminance at the same driving voltage is found to be significantly increased, albeit the independent current density (Figures 4E and S13A), leading to PE improvement (Figures 4F and S13C). With the white device containing 0.7 wt.% Ir(Flpy-CF_3)$_3$ as an example, the maximum luminance is from 23,085 to 44,485 cd m^{-2} accompanied by the enhanced maximum PE from 68.5 to 130.1 lm W^{-1} (Table 2). Noticeably, the PE at a high luminance of 1,000 and 5,000 cd m^{-2} could also reach up to 96.3 and 69.0 lm W^{-1}, respectively. These values are the highest ever reported for s-WOLEDs, which are comparable to those of v-WOLEDs and even competent with the commercial fluorescent tubes (Table 3). Interestingly, the related

correlated color temperature and CIE coordinates can be well tuned to satisfy different illumination requirements without considerably sacrificing the PE (Figure S15 and Table S4).

Conclusion

In summary, we report power-efficient s-WOLEDs with PE approaching 100 lm W^{-1} at l,000 cd m^{-2} luminance. This is obtained by newly developing a high-energy-level blue phosphor FIr-*p*-OC_8 in combination with the dendritic host H2, where hole scattering can be eliminated to allow the direct formation of excitons. As a result, the solution-processed white-light-emitting device based on FIr-*p*-OC_8 realizes a record-high PE of 68.5 lm W^{-1} at the maximum and 47.0 lm W^{-1} at a practical luminance of 1,000 cd m^{-2}, which can be further improved to 130.1 and 96.3 lm W^{-1}, respectively, under light outcoupling. We believe that our work represents an important progress in s-WOLEDs and demonstrates their bright future in low-cost, large-area, and flexible energy-saving lightings.

METHODS

All methods can be found in the accompanying Transparent Methods supplemental file.

SUPPLEMENTAL INFORMATION

Supplemental Information includes Transparent Methods, 15 figures, 4 tables, and 1 scheme and can be found with this article online at https://doi.org/10.1016/j.isci.2018.07.016.

ACKNOWLEDGMENTS

The authors thank Liping Zhu for assisting transient EL measurement. S.W., B.Z., J.D., Z. X., and L.W. acknowledge financial support from the National Key Basic Research and Development Program of China (973 program, Grant No. 2015CB65001), founded by MOST, and the National Natural Science Foundation of China (Grant Nos. 91333205, 51573183, 51322308, 51473162, 51325303, and 51703223). W.-Y.W. acknowledges financial support from the Hong Kong Polytechnic University (1-ZE1C); Ms Clarea Au for the Endowed Professorship (847S); Areas of Excellence Scheme, University Grants Committee of HKSAR, China (AoE/P-03/08); and Hong Kong Research Grants Council (HKBU 12304715).

AUTHOR CONTRIBUTIONS

J.D. and L.W. coordinated and directed the study. S.W., B.Z., and J.D. conceived the idea and designed the experiments. S.W. fabricated and characterized the devices. L.Z. synthesized the blue phosphors FIr-*m*-OC_8 and FIr-*p*-OC_8. W.-Y.W. provided the yellow phosphor Ir(FIpy-CF_3)$_3$. Z.X. helped to design device structures and took part in discussions about the device results. S.W., B.Z., J.D., L.W., and W.-Y.W. wrote and revised the manuscript.

DECLARATION OF INTERESTS

The authors declare no competing interests.

Received: April 6, 2018
Revised: June 19, 2018
Accepted: July 19, 2018
Published: August 31, 2018

REFERENCES

Aizawa, N., Pu, Y.-J., Watanabe, M., Chiba, T., Ideta, K., Toyota, N., Igarashi, M., Suzuri, Y., Sasabe, H., and Kido, J. (2014). Solution-processed multilayer small-molecule light-emitting devices with high-efficiency white-light emission. Nat. Commun. *5*, 5756.

Chang, Y.-L., Yin, S., Wang, Z., Helander, M.G., Qiu, J., Chai, L., Liu, Z., Scholes, G.D., and Lu, Z. (2013). Highly efficient warm white organic light-emitting diodes by triplet exciton conversion. Adv. Funct. Mater. *23*, 705–712.

Chiba, T., Pu, Y.-J., and Kido, J. (2015). Solution-processed white phosphorescent tandem organic light-emitting devices. Adv. Mater. *27*, 4681–4687.

Ding, J., Zhang, B., Lu, J., Xie, Z., Wang, L., Jing, X., and Wang, F. (2009). Solution-processable carbazole-based conjugated dendritic hosts for power-efficient blue-electrophosphorescent devices. Adv. Mater. *21*, 4983–4986.

Ding, L., Dong, S., Jiang, Z., Chen, H., and Liao, L. (2015). Orthogonal molecular structure for better host material in blue phosphorescence and larger OLED white lighting panel. Adv. Funct. Mater. *25*, 645–650.

Fu, Q., Chen, J., Shi, C., and Ma, D. (2012). Solution-processed small molecules as mixed host for highly efficient blue and white phosphorescent organic light-emitting diodes. ACS Appl. Mater. Interfaces *4*, 6579–6586.

Huang, F., Shih, P.I., Shu, C.F., Chi, Y., and Jen, A.K.Y. (2009). Highly efficient polymer white-light-emitting diodes based on lithium salts doped

electron transporting layer. Adv. Mater. *21*, 361–365.

Kamtekar, K.T., Monkman, A.P., and Bryce, M.R. (2010). Recent advances in white organic light-emitting materials and devices (WOLEDs). Adv. Mater. *22*, 572–582.

Kido, J., Kimura, M., and Nagai, K. (1995). Multilayer white light-emitting organic electroluminescent device. Science *267*, 1332–1334.

Lee, C.W., and Lee, J.Y. (2013). High quantum efficiency in solution and vacuum processed blue phosphorescent organic light emitting diodes using a novel benzofuropyridine-based bipolar host material. Adv. Mater. *25*, 596–600.

Lee, J.-H., Cheng, S.-H., Yoo, S.-J., Shin, H., Chang, J.-H., Wu, C.-I., Wong, K.-T., and Kim, J.-J. (2015). An exciplex forming host for highly efficient blue organic light emitting diodes with low driving voltage. Adv. Funct. Mater. *25*, 361–366.

Li, B., Chen, J., Zhao, Y., Yang, D., and Ma, D. (2011). Effects of carrier trapping and scattering on hole transport properties of N,N′-diphenyl-N,N′-bis(1-naphthyl)-1,1′-biphenyl-4,4′-diamine thin films. Org. Electron. *12*, 974–979.

Li, B., Chen, J., Yang, D., Zhao, Y., and Ma, D. (2012a). The effects of tris(2-phenylpyridine) iridium on the hole injection and transport properties of 4,4′,4′-tri(N-carbazolyl)-triphenylamine thin films. Thin Solid Films *522*, 352–356.

Li, C., Duan, L., Sun, Y., Li, H., and Qiu, Y. (2012b). Charge transport in mixed organic disorder semiconductors: trapping, scattering, and effective energetic disorder. J. Phys. Chem. C *116*, 19748–19754.

Li, C., Duan, L., Li, H., and Qiu, Y. (2014). Universal trap effect in carrier transport of disordered organic semiconductors: transition from shallow trapping to deep trapping. J. Phys. Chem. C *118*, 10651–10660.

Liu, R., Gan, Z., Shinar, R., and Shinar, J. (2011). Transient electroluminescence spikes in small molecular organic light-emitting diodes. Phys. Rev. B *83*, 245302.

Liu, B., Nie, H., Zhou, X., Hu, S., Luo, D., Gao, D., Zou, J., Xu, M., Wang, L., Zhao, Z., et al. (2016). Manipulation of charge and exciton distribution based on blue aggregation-induced emission fluorophors: a novel concept to achieve high-performance hybrid white organic light-emitting diodes. Adv. Funct. Mater. *26*, 776–783.

Ou, Q.-D., Zhou, L., Li, Y.-Q., Shen, S., Chen, J.-D., Li, C., Wang, Q.-K., Lee, S.-T., and Tang, J.-X. (2014). Extremely efficient white organic light-emitting diodes for general lighting. Adv. Funct. Mater. *24*, 7249–7256.

Park, Y.-S., Kang, J.-W., Kang, D.M., Park, J.-W., Kim, Y.-H., Kwon, S.-K., and Kim, J.-J. (2008). Efficient, color stable white organic light-emitting diode based on high energy level yellowish-green dopants. Adv. Mater. *20*, 1957–1961.

Park, Y.-S., Lee, S., Kim, K.-H., Kim, S.-Y., Lee, J.-H., and Kim, J.-J. (2013). Exciplex-forming co-host for organic light-emitting diodes with ultimate efficiency. Adv. Funct. Mater. *23*, 4914–4920.

Reineke, S., Lindner, F., Schwartz, G., Seidler, N., Walzer, K., Lüssem, B., and Leo, K. (2009). White organic light-emitting diodes with fluorescent tube efficiency. Nature *459*, 234–238.

Schmechel, R., and von Seggern, H. (2004). Electronic traps in organic transport layers. Phys. Status Solidi A *201*, 1215–1235.

Seino, Y., Sasabe, H., Pu, Y.-J., and Kido, J. (2014). High-performance blue phosphorescent OLEDs using energy transfer from exciplex. Adv. Mater. *26*, 1612–1616.

Su, S., Gonmori, E., Sasabe, H., and Kido, J. (2008). Highly efficient organic blue- and white-light-emitting devices having a carrier- and exciton-confining structure for reduced efficiency roll-off. Adv. Mater. *20*, 4189–4194.

Sun, Y., Giebink, N.C., Kanno, H., Ma, B., Thompson, M.E., and Forrest, S.R. (2006). Management of singlet and triplet excitons for efficient white organic light-emitting devices. Nature *440*, 908–912.

Tong, K.L., Tsang, S.W., Tsung, K.K., Tse, S.C., and So, S.K. (2007). Hole transport in molecularly doped naphthyl diamine. J. Appl. Phys. *102*, 093705.

Tsung, K.K., and So, S.K. (2008). Carrier trapping and scattering in amorphous organic hole transporter. Appl. Phys. Lett. *92*, 103315.

von Malm, N., Steiger, J., Schmechel, R., and von Seggern, H. (2001). Trap engineering in organic hole transport materials. J. Appl. Phys. *89*, 5559–5563.

Wang, Q., Ding, J., Ma, D., Cheng, Y., Wang, L., and Wang, F. (2009). Manipulating charges and excitons within a single-host system to accomplish efficiency/CRI/color-stability trade-off for high-performance OWLEDs. Adv. Mater. *21*, 2397–2401.

Wang, Z., Helander, M., Qiu, J., Puzzo, D., Greiner, M., Liu, Z., and Lu, Z. (2011). Highly simplified phosphorescent organic light emitting diode with > 20% external quantum efficiency at > 10,000 cd/m^2. Appl. Phys. Lett. *98*, 073310.

Wang, S., Zhang, B., Wang, X., Ding, J., Xie, Z., and Wang, L. (2015). Ultrahigh color-stable, solution-processed, white OLEDs using a dendritic binary host and long-wavelength dopants with different charge trapping depths. Adv. Opt. Mater. *3*, 1349–1354.

Weichsel, C., Burtone, L., Reineke, S., Hintschich, S.I., Gather, M.C., Leo, K., and Lüssem, B. (2012). Storage of charge carriers on emitter molecules in organic light-emitting diodes. Phys. Rev. B *86*, 075204.

Wu, H., Zou, J., Liu, F., Wang, L., Mikhailovsky, A., Bazan, G.C., Yang, W., and Cao, Y. (2008). Efficient single active layer electrophosphorescent white polymer light-emitting diodes. Adv. Mater. *20*, 696–702.

Wu, H., Zhou, G., Zou, J., Ho, C.-L., Wong, W.-Y., Yang, W., Peng, J., and Cao, Y. (2009). Efficient polymer white-light-emitting devices for solid-state lighting. Adv. Mater. *21*, 4181–4184.

Wu, S.F., Li, S.H., Sun, Q., Huang, C.C., and Fung, M.K. (2016). Highly efficient white organic light-emitting diodes with ultrathin emissive layers and a spacer-free structure. Sci. Rep. *6*, 25821.

Wu, S.F., Li, S.H., Wang, Y.K., Huang, C.C., Sun, Q., Liang, J.J., Liao, L.S., and Fung, M.K. (2017). White organic LED with a luminous efficacy exceeding 100 lm W^{-1} without light out-coupling enhancement techniques. Adv. Funct. Mater. *27*, 1701314.

Zhang, B., Tan, G., Lam, C.-S., Yao, B., Ho, C.-L., Liu, L., Xie, Z., Wong, W.-Y., Ding, J., and Wang, L. (2012). High-efficiency single emissive layer white organic light-emitting diodes based on solution-processed dendritic host and new orange-emitting iridium complex. Adv. Mater. *24*, 1873–1877.

Zhang, B., Liu, L., Tan, G., Yao, B., Ho, C.-L., Wang, S., Ding, J., Xie, Z., Wong, W.-Y., and Wang, L. (2013). Interfacial triplet confinement for achieving efficient solution-processed deep-blue and white electrophosphorescent devices with underestimated poly(N-vinylcarbazole) as the host. J. Mater. Chem. C *1*, 4933–4939.

Zhou, L., Ou, Q.-D., Li, Y.-Q., Xiang, H.-Y., Xu, L.-H., Chen, J.-D., Li, C., Shen, S., Lee, S.-T., and Tang, J.-X. (2015). Efficiently releasing the trapped energy flow in white organic light-emitting diodes with multifunctional nanofunnel arrays. Adv. Funct. Mater. *25*, 2660–2668.

Zhu, L., Zhao, Y., Zhang, H., Chen, J., and Ma, D. (2014). Using an ultra-thin non-doped orange emission layer to realize high efficiency white organic light-emitting diodes with low efficiency roll-off. J. Appl. Phys. *115*, 244512.

Zhu, L., Wu, Z., Chen, J., and Ma, D. (2015). Reduced efficiency roll-off in all-phosphorescent white organic light-emitting diodes with an external quantum efficiency of over 20%. J. Mater. Chem. C *3*, 3304–3310.

Zou, J., Wu, H., Lam, C.-S., Wang, C., Zhu, J., Zhong, C., Hu, S., Ho, C.-L., Zhou, G.-J., Wu, H., et al. (2011). Simultaneous optimization of charge-carrier balance and luminous efficacy in highly efficient white polymer light-emitting devices. Adv. Mater. *23*, 2976–2980.

ISCI, Volume *6*

Supplemental Information

High-Energy-Level Blue Phosphor for Solution-Processed White Organic Light-Emitting Diodes with Efficiency Comparable to Fluorescent Tubes

Shumeng Wang, Lei Zhao, Baohua Zhang, Junqiao Ding, Zhiyuan Xie, Lixiang Wang, and Wai-Yeung Wong

Supplemental Schemes

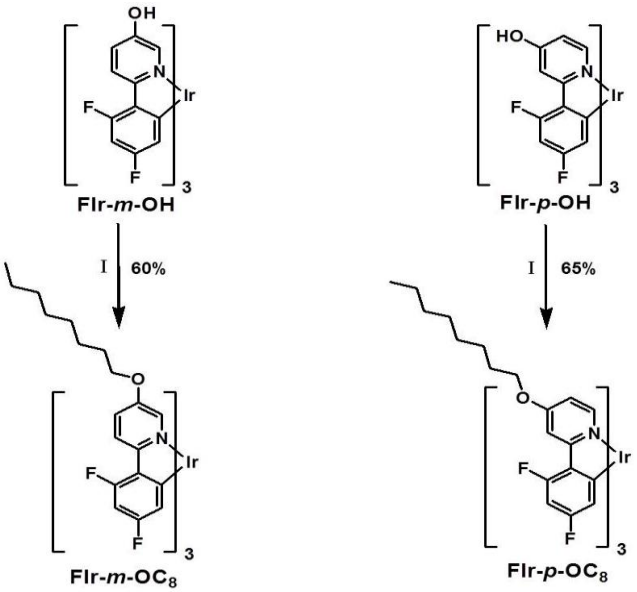

Scheme S1. Synthesis of the iridium complexes FIr-*m*-OC$_8$ and FIr-*p*-OC$_8$. Reagents and conditions: I) Cs_2CO_3, DMF, alkyl bromide, 70 ℃, 6 h. Related to Figure 1.

Synthesis of the iridium complexes FIr-*m*-OC$_8$ and FIr-*p*-OC$_8$.

All solvents for chemical synthesis were purified according to the standard procedures. FIr-*m*-OH and FIr-*p*-OH were prepared according to the literature methods (Wang et al., 2015; Wang et al., 2016). **FIr-*m*-OC$_8$**: To a solution of FIr-*m*-OH (0.40 g, 1 mmol) and Cs_2CO_3 (1.08 g, 3.3 mmol) in DMF (15 mL) was added butyl bromide (0.48 g, 3.5 mmol). After being heated at 70 ^oC for 6 h, the mixture was poured into water, and extracted with dichloromethane. The organic layer was carefully washed with water and dried with anhydrous Na_2SO_4. After the solvent was removed, the residue was isolated by using silica gel column chromatography (petroleum ether/dichloromethane = 3/1, v/v) to give a pure product (0.68 g, 70 %). ^1H NMR (400 MHz, $CDCl_3$) δ 8.19 (dd, *J* = 9.2, 2.5 Hz, 3H), 7.26 - 7.22 (m, 3H), 7.13 (d, *J* = 2.8 Hz, 3H), 6.37 (ddd, *J* = 12.8, 9.0, 2.4 Hz, 3H), 6.21 (dd, *J* = 9.2, 2.4 Hz, 3H), 4.05 (t, *J* = 6.4 Hz, 6H), 2.03 - 1.62 (m, 6H), 1.63 - 1.39 (m, 6H), 1.31 (dd, *J* = 13.9, 7.7 Hz, 24H), 0.89 (t, *J* = 6.7 Hz, 9H). ^{19}F NMR (376 MHz, $CDCl_3$, δ (vs. fluorobenzene)): 2.58 (d, *J* = 9.3Hz, 3F), -0.11 (d, *J* = 9.2Hz, 3F). MS (MALDI-TOF) *m/z*: 979.3 [M^+]. Anal. Calcd for $C_{57}H_{66}F_6IrN_3O_3$: C 59.67, H 5.80, N 3.66 Found C 59.70, H 5.83, N 3.65. **FIr-*p*-OC$_8$**: This compound was prepared from FIr-*p*-OH and octyl bromide according to a similar procedure as FIr-*m*-OC$_8$. Silica gel column chromatography (petroleum ether/dichloromethane = 3/1, v/v) was applied to provide the desired product as a yellow solid (0.75 g, 65 %).^1H NMR (400 MHz, $CDCl_3$) δ 7.77 (t, *J* = 3.0 Hz, 3H), 7.27 (d, *J* = 3.2 Hz, 3H), 6.47 (dd, *J* = 6.4, 2.5 Hz, 3H), 6.41 - 6.30 (m, 3H), 6.25 (dd, *J* = 9.2, 2.3 Hz, 3H), 4.03 (t, *J* = 6.4 Hz, 6H), 2.03 - 1.62 (m, 6H), 1.63 - 1.39 (m, 6H), 1.31 (dd, *J* = 13.9, 7.7 Hz, 24H), 0.88 (t, *J* = 6.7 Hz, 9H). ^{19}F NMR (376 MHz, $CDCl_3$, δ (vs. fluorobenzene)): 3.70 (d, *J* = 9.7 Hz, 3F), 1.89 (d, *J* = 9.7 Hz, 3F). MS (MALDI-TOF) *m/z*: 1147.4 [M^+]. Anal. Calcd for $C_{57}H_{66}F_6IrN_3O_3$: C 59.67, H 5.80, N 3.66 Found: C 59.70, H 5.83, N 3.65.

Supplemental Figures

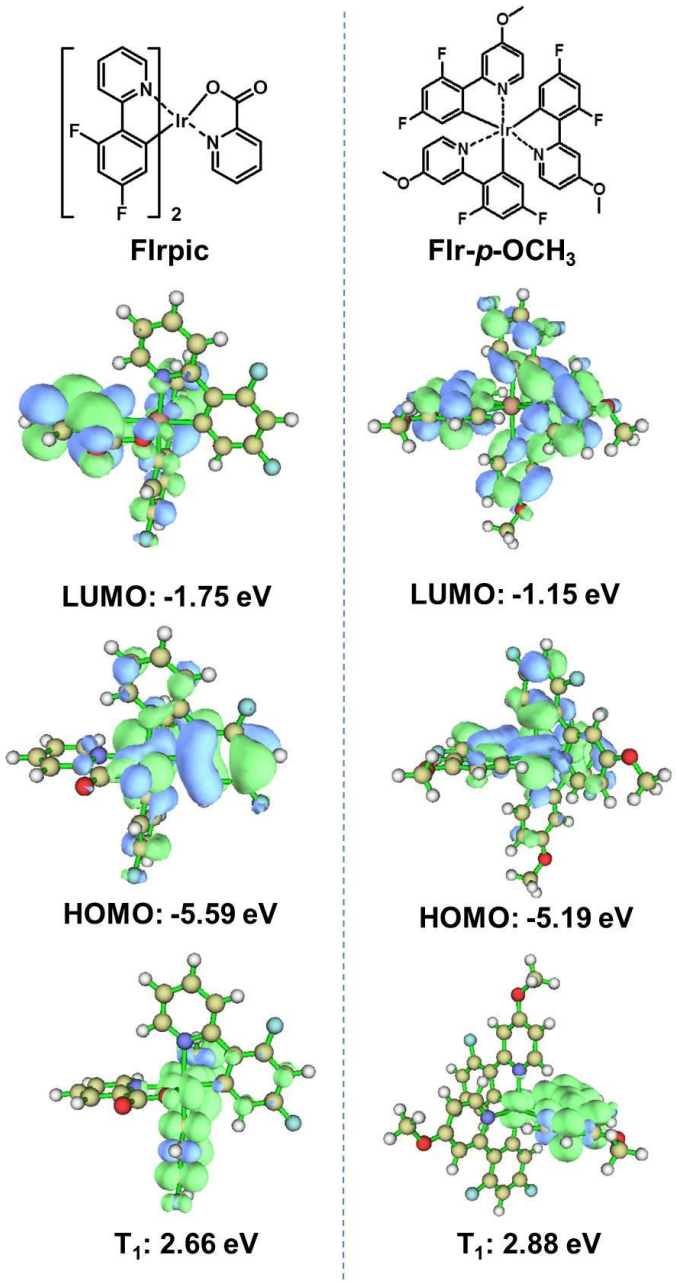

Figure S1. Distribution of HOMO/LUMO and triplet molecular orbitals. For simplicity, methoxyl is used for blue phosphor. Data were calculated by TD-DFT (Gaussian 09, B3LYP, 6-31G*). Related to Figure 1.

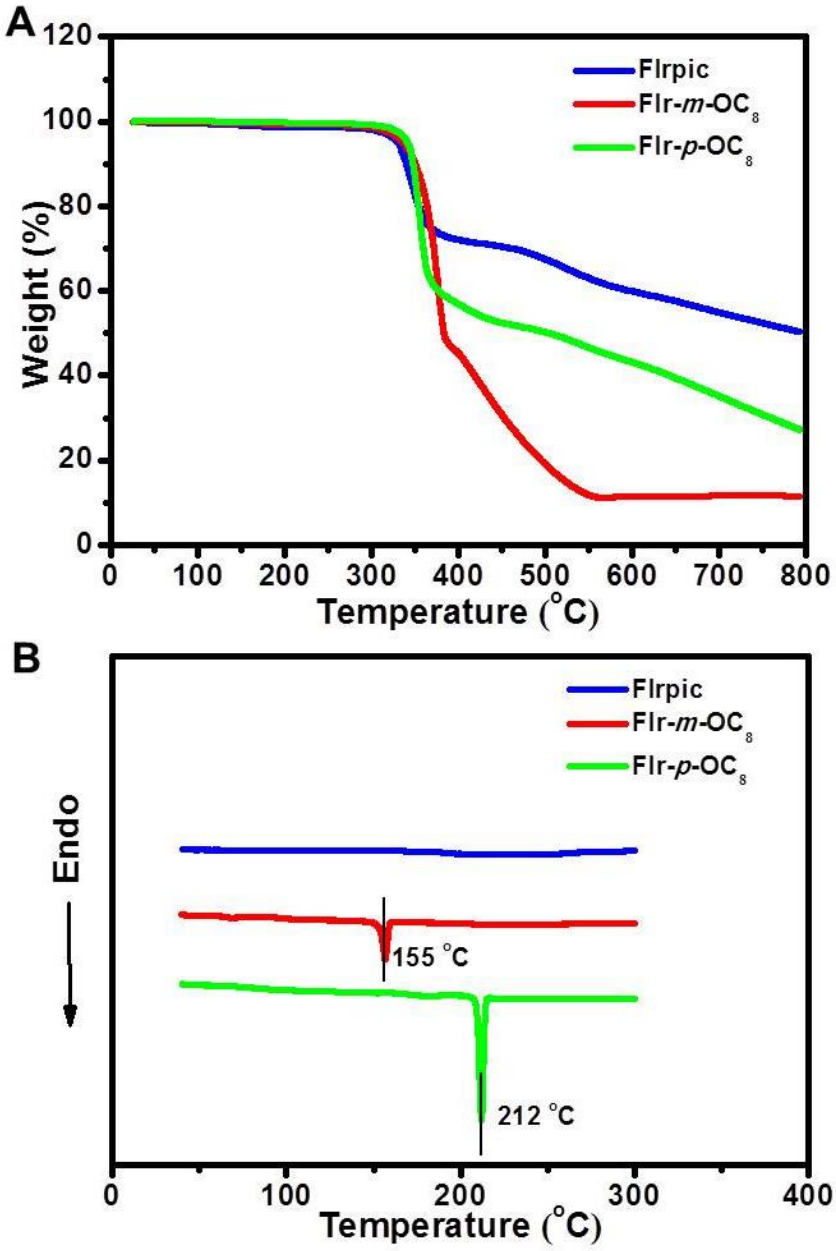

Figure S2. (**A**) TGA spectra for the blue phosphors at a heating rate of 10 ^{o}C/min under N2; (**B**) DSC spectra of the second heating cycling for the blue phosphors at a heating rate of 10 ^{o}C min^{-1} under N_2. Related to Table 1.

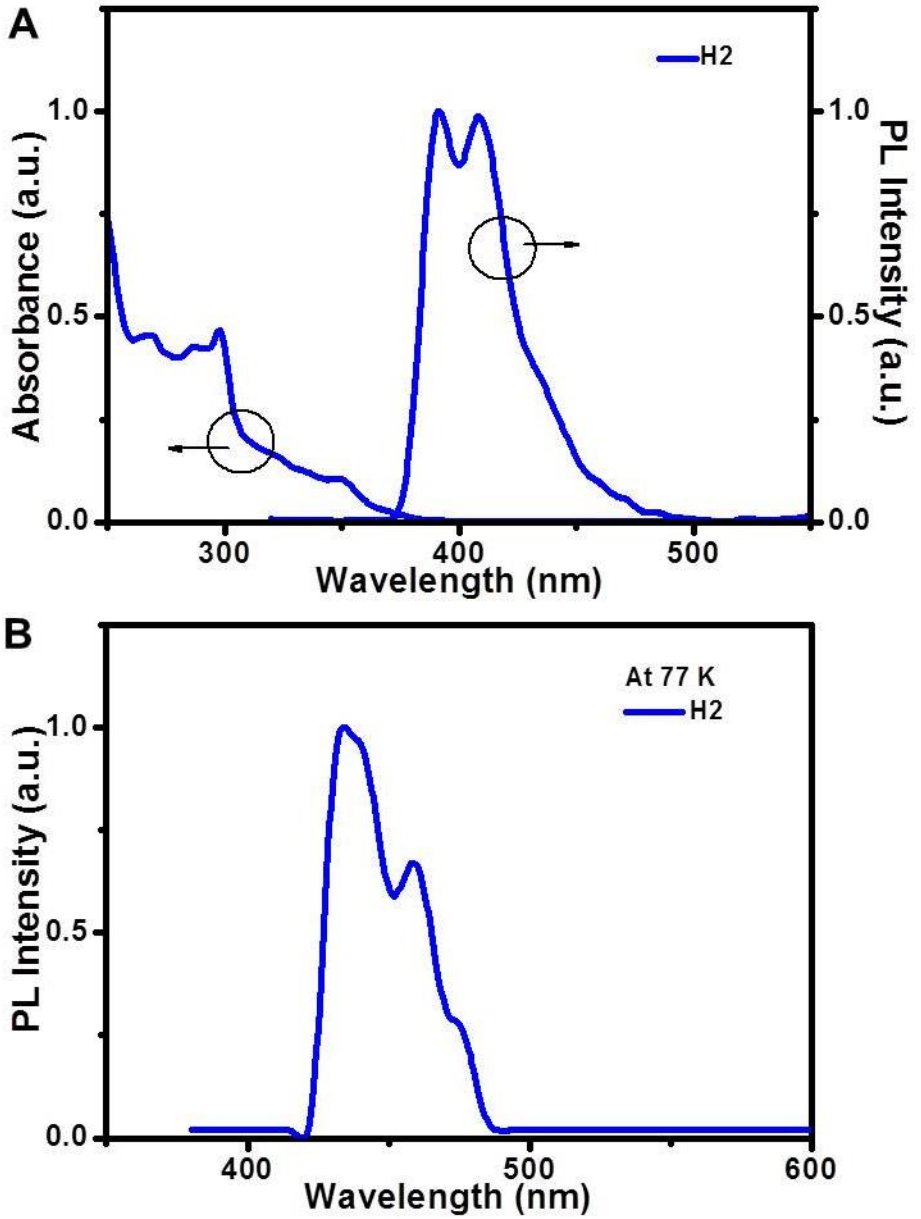

Figure S3. (**A**) UV-Vis absorption spectra in DCM together with PL spectra in toluene of H2. (**B**) Phosphorescent spectra of H2 in toluene solution (5×10^{-4}M) at 77K. Related to Table 1.

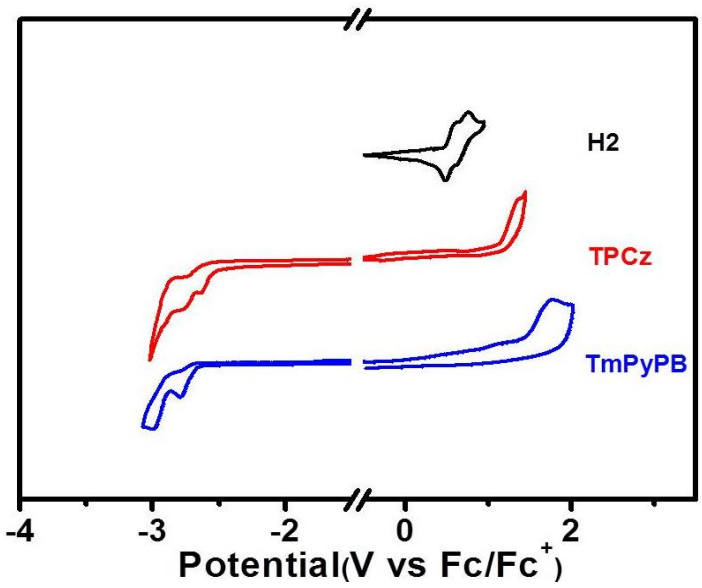

Figure S4. Cyclic voltammograms of host and electron transporting materials. H2, TPCz and TmPyPB in solution using 0.1M n-Bu_4NClO_4 as supporting electrolyte at a scan rate of 100 mV s^{-1}. Related to Table 1 and Figure 3.

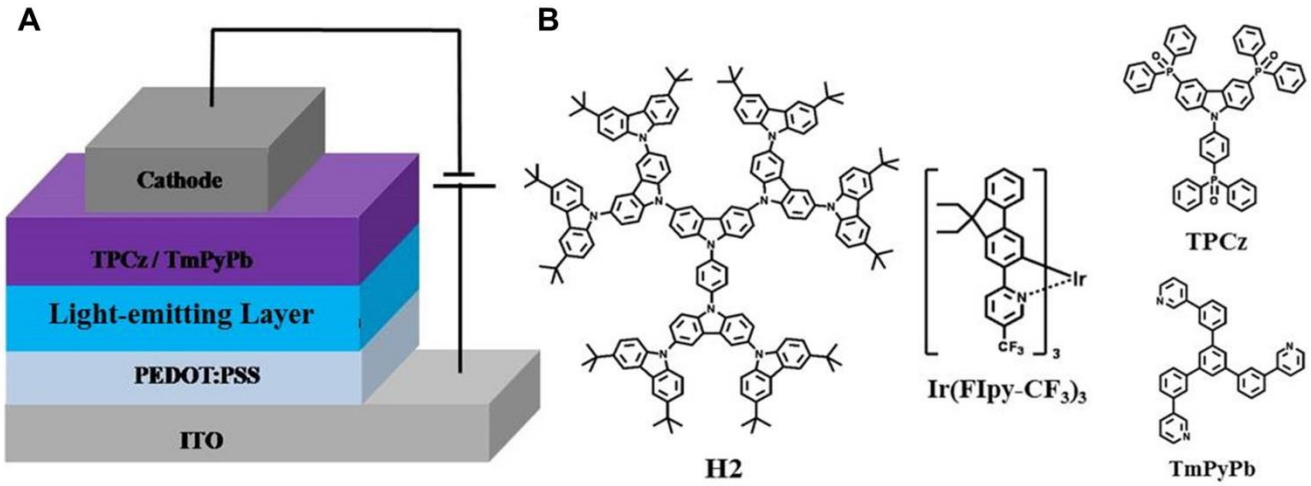

Figure S5. Device configuration and the structure of the materials. (**A**) Device configuration, in which the light-emitting layer is H2:Blue phosphor for blue devices and H2:Blue phosphor:Ir(Flpy-CF_3)$_3$ for white devices. (**B**) Molecular structures of the used materials including yellow phosphor (Ir(Flpy-CF_3)$_3$), hole blocking and electron transporting materials (TPCz and TmPyPB), and dendritic host (H2). Related to Figure 2 and Figure 4.

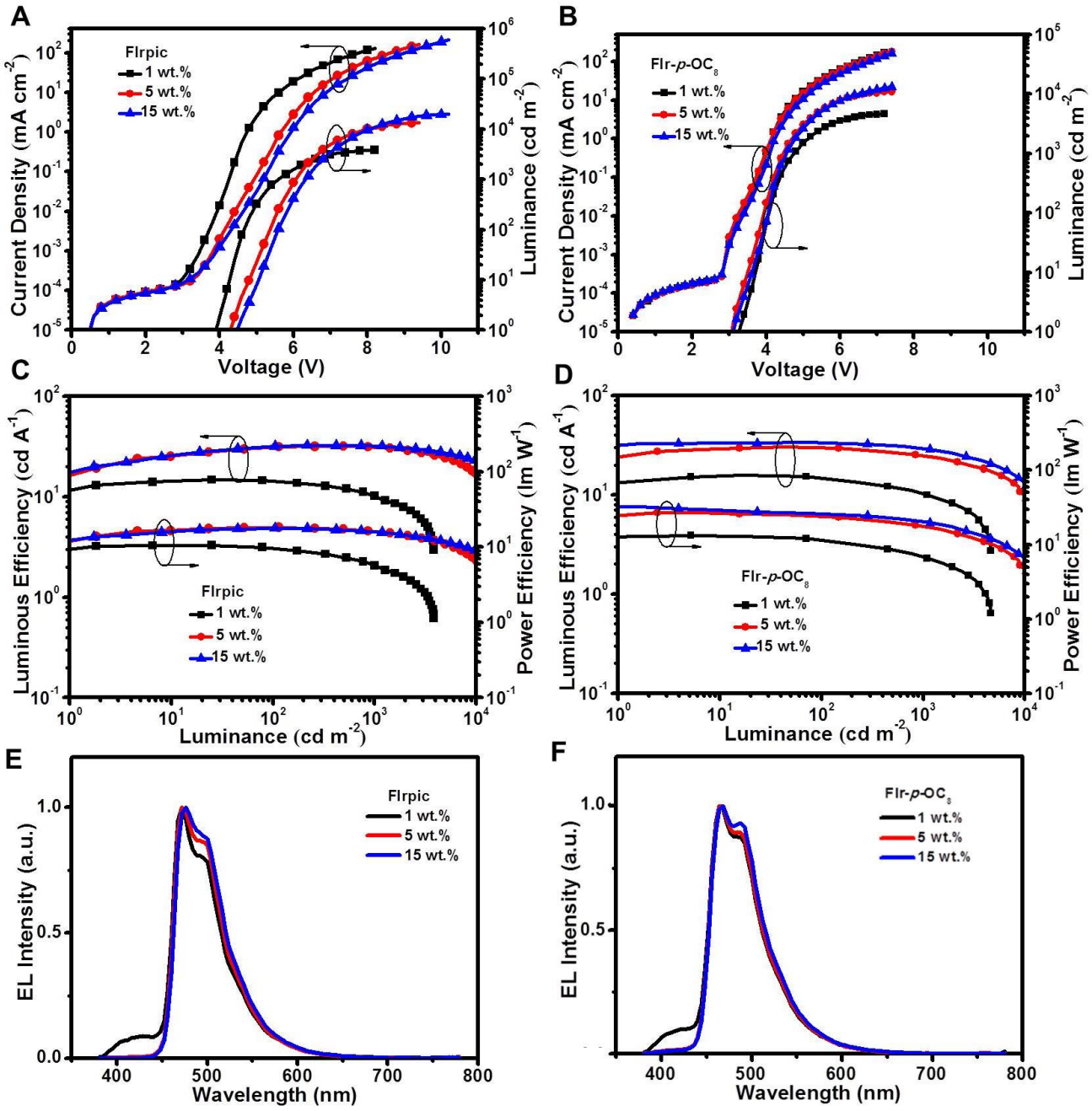

Figure S6. Performance of FIrpic and Flr-*p*-OC$_8$ based blue devices with different doping concentration. Current density - voltage-luminance characteristics (**A** and **B**), current efficiency - luminance - power efficiency characteristics (**C** and **D**), and EL spectra (**E** and **F**) for FIrpic and Flr-*p*-OC$_8$ based blue devices, respectively. Related to Figure 2.

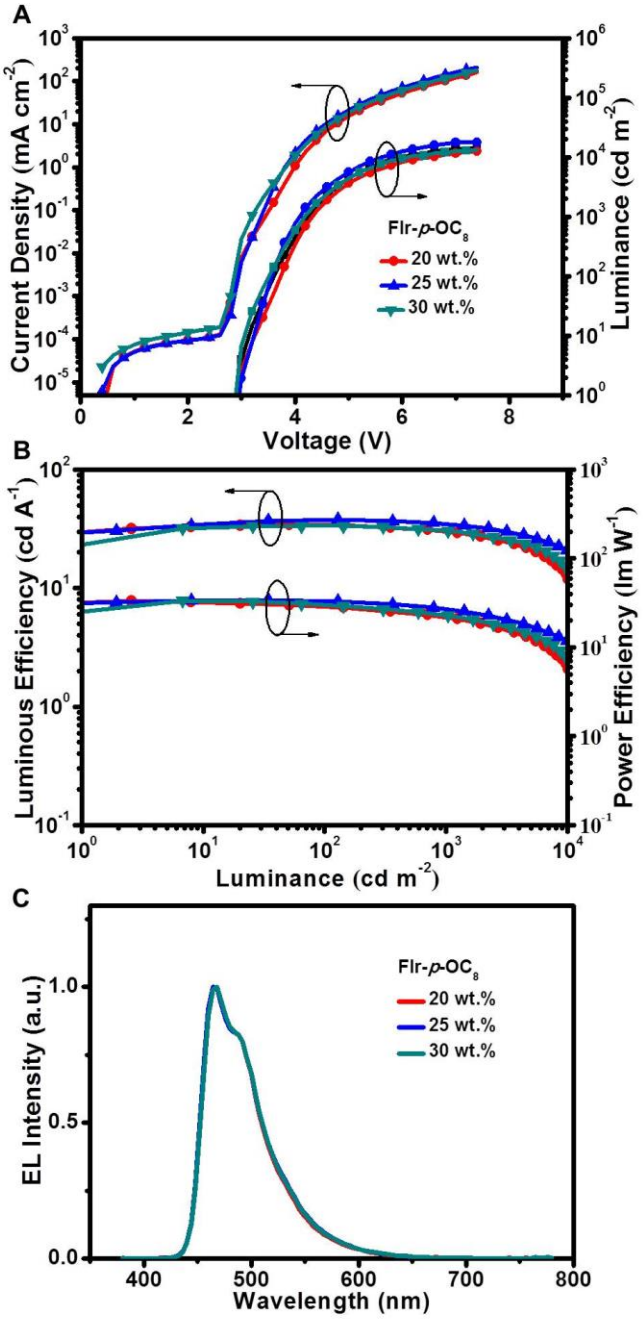

Figure S7. Performance of FIr-*p*-OC$_8$ based blue devices with high doping concentration. Current density - voltage - luminance characteristics (**A**), luminous efficiency - luminance - power efficiency characteristics (**B**), and EL spectra (**C**) for FIr-*p*-OC$_8$ based blue emitting device with high doping concentration. Related to Figure 4.

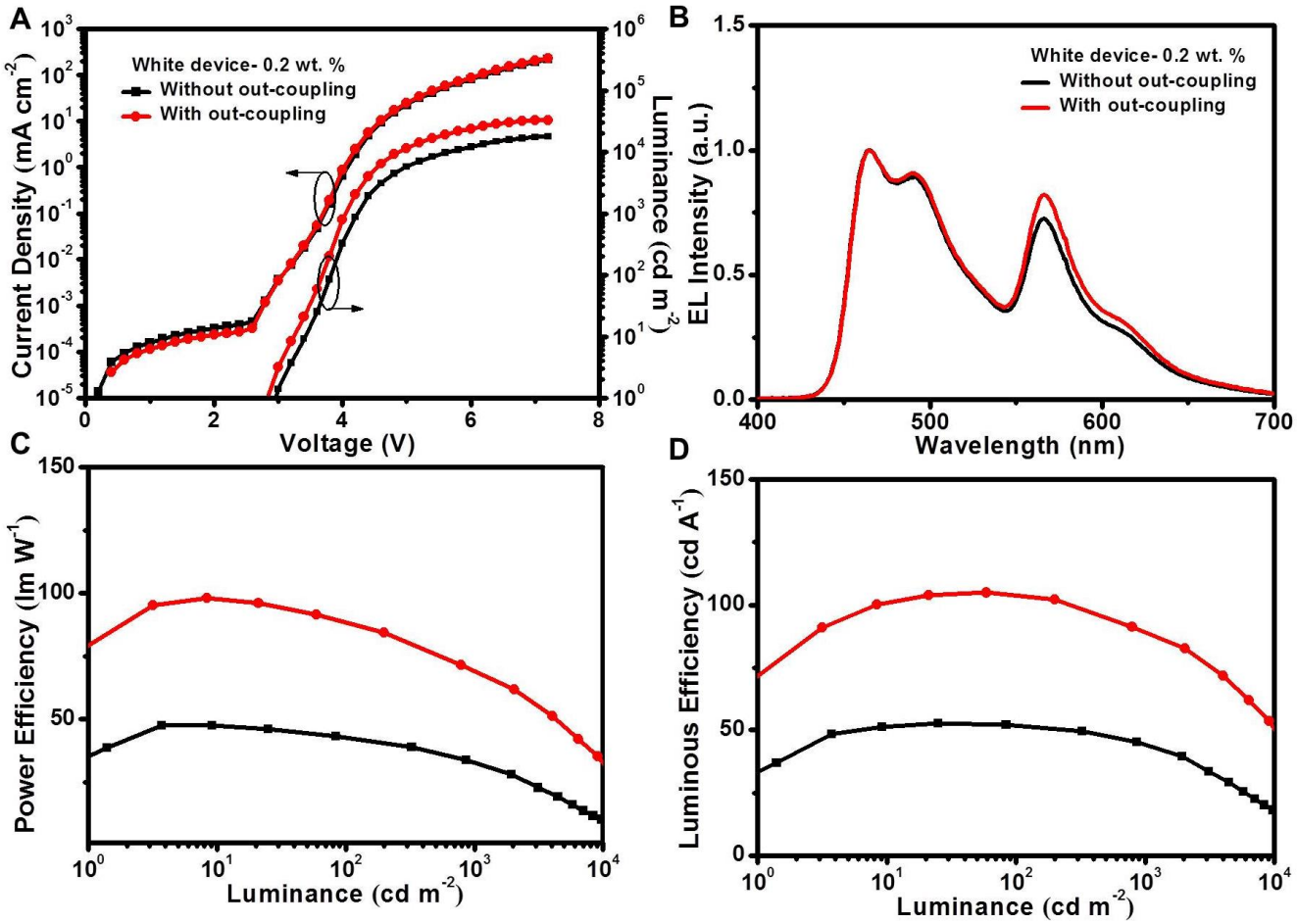

Figure S8. Performance of FIr-*p*-OC_8 based white device with a 0.2 wt.% content of Ir(FIpy-CF_3)$_3$. (**A**) Current density-voltage-luminance characteristics. (**B**) EL spectra at 1000 cd m^{-2}. (**C**) Power efficiency as a function of luminance. (**D**) Luminous efficiency as a function of luminance. Related to Figure 4.

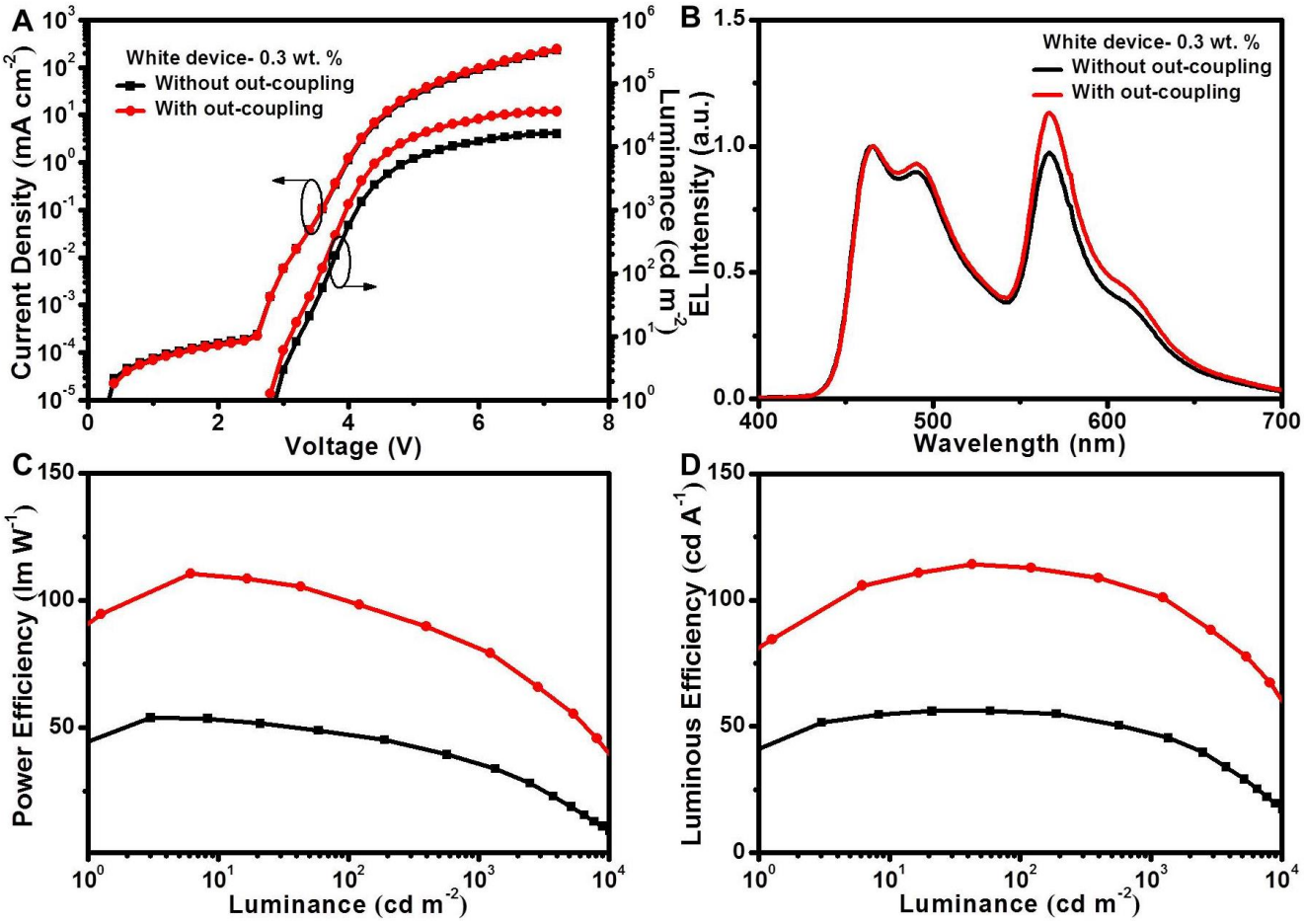

Figure S9. Performance of FIr-*p*-OC_8 based white device with a 0.3 wt.% content of Ir(FIpy-CF_3)$_3$. (**A**) Current density-voltage-luminance characteristics. (**B**) EL spectra at 1000 cd m^{-2}. (**C**) Power efficiency as a function of luminance. (**D**) Luminous efficiency as a function of luminance. Related to Figure 4.

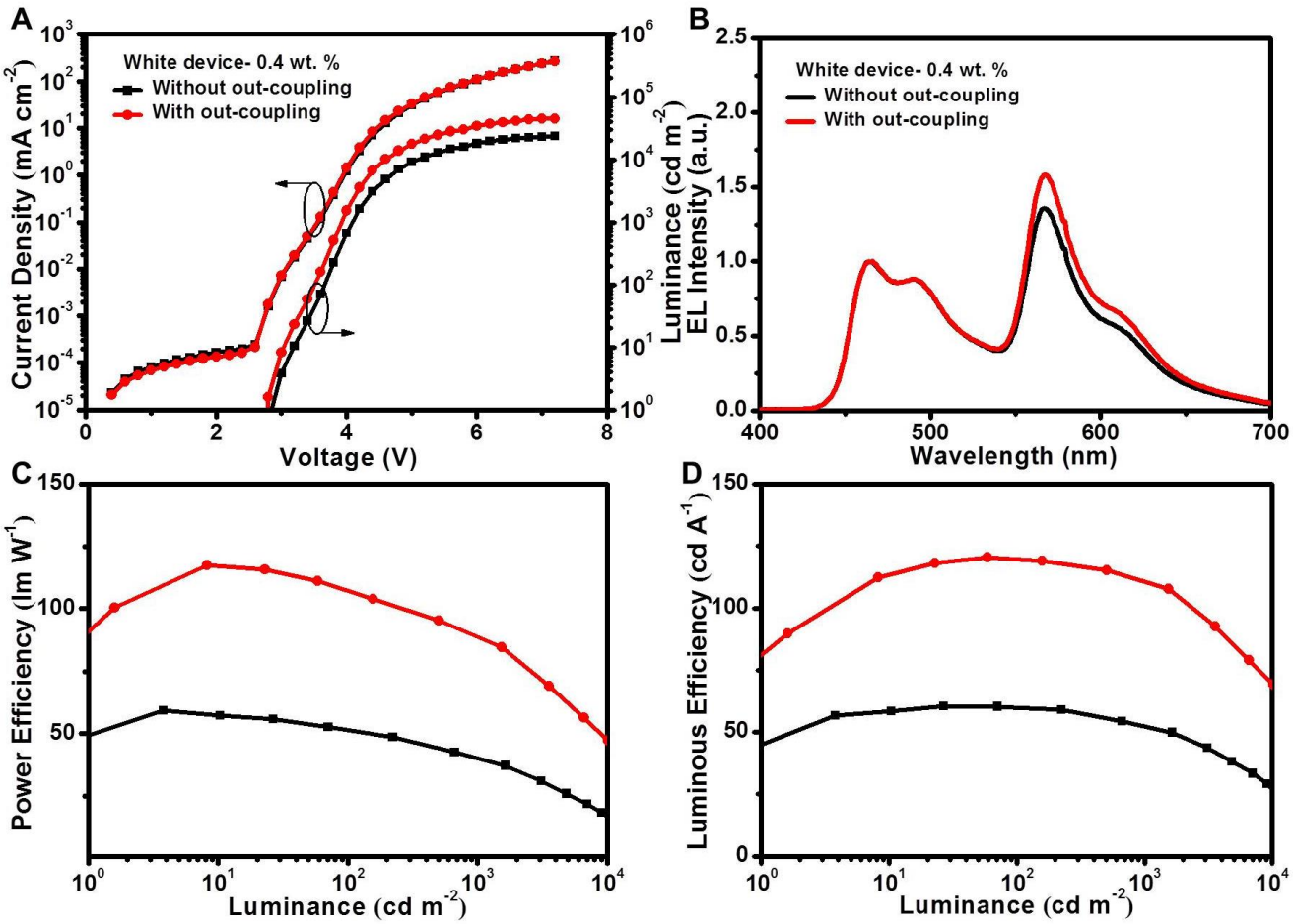

Figure S10. Performance of FIr-*p*-OC_8 based white device with a 0.4 wt.% content of Ir(FIpy-CF_3)$_3$. (**A**) Current density-voltage-luminance characteristics. (**B**) EL spectra at 1000 cd m^{-2}. (**C**) Power efficiency as a function of luminance. (**D**) Luminous efficiency as a function of luminance. Related to Figure 4 and Table 2.

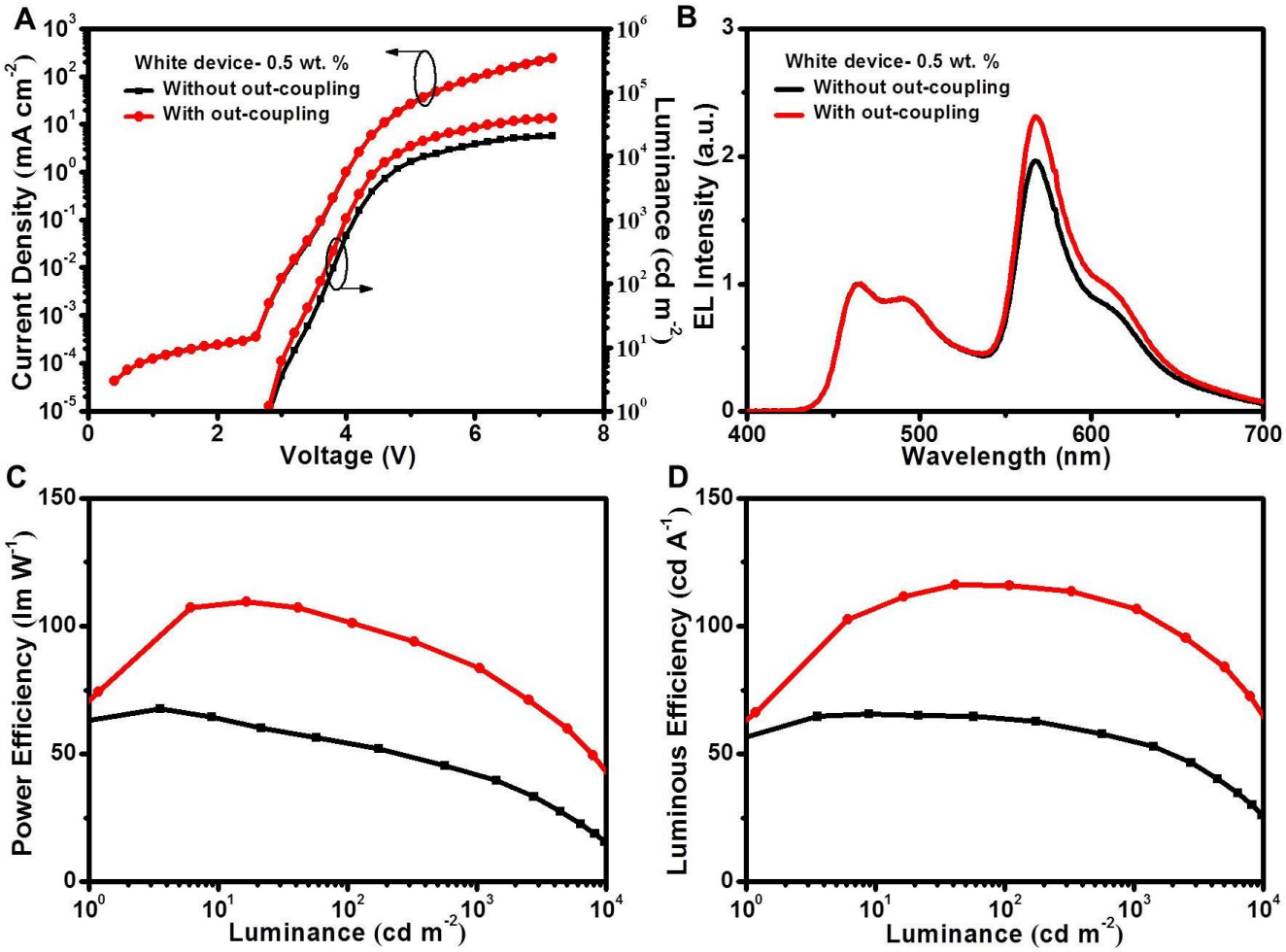

Figure S11. Performance of FIr-*p*-OC_8 based white device with a 0.5 wt.% content of Ir(FIpy-CF_3)$_3$. (**A**) Current density-voltage-luminance characteristics. (**B**) EL spectra at 1000 cd m^{-2}. (**C**) Power efficiency as a function of luminance. (**D**) Luminous efficiency as a function of luminance. Related to Figure 4.

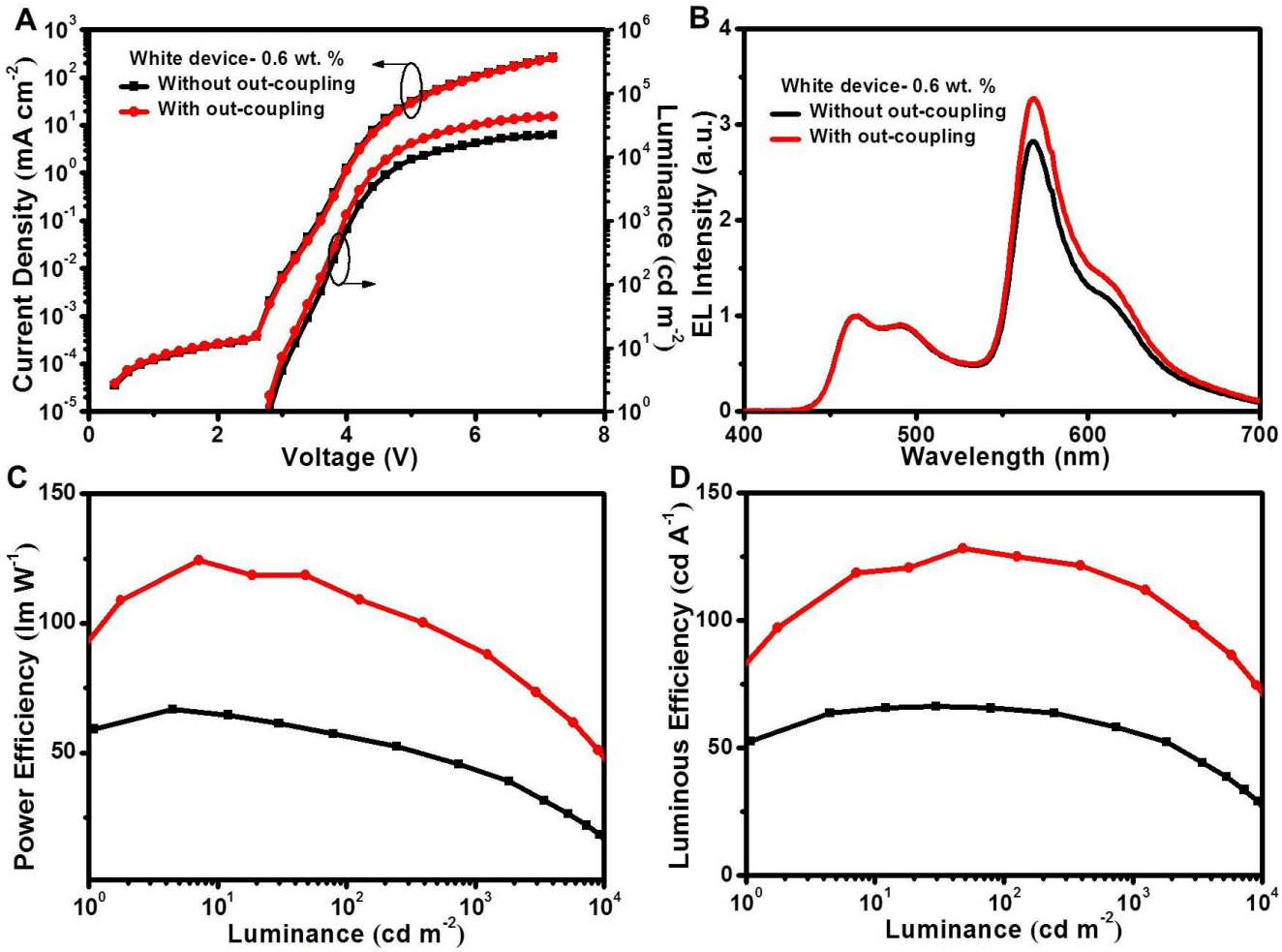

Figure S12. Performance of FIr-*p*-OC_8 based white device with a 0.6 wt.% content of Ir(Flpy-CF_3)$_3$. (**A**) Current density-voltage-luminance characteristics. (**B**) EL spectra at 1000 cd m^{-2}. (**C**) Power efficiency as a function of luminance. (**D**) Luminous efficiency as a function of luminance. Related to Figure 4.

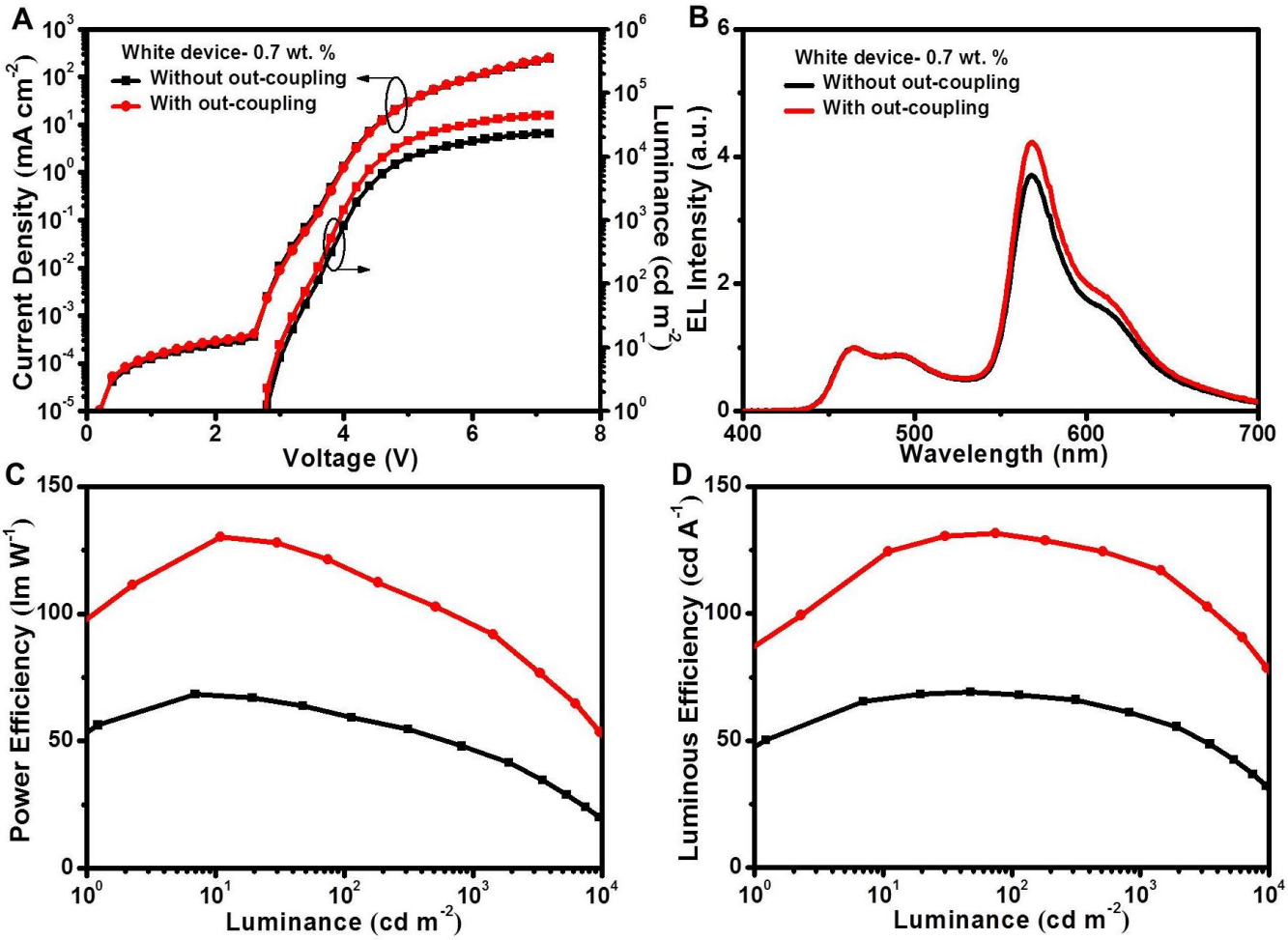

Figure S13. Performance of FIr-*p*-OC_8 based white device with a 0.7 wt.% content of Ir(FIpy-CF_3)$_3$. (**A**) Current density-voltage-luminance characteristics. (**B**) EL spectra at 1000 cd m^{-2}. (**C**) Power efficiency as a function of luminance. (**D**) Luminous efficiency as a function of luminance. Related to Figure 4 and Table 2.

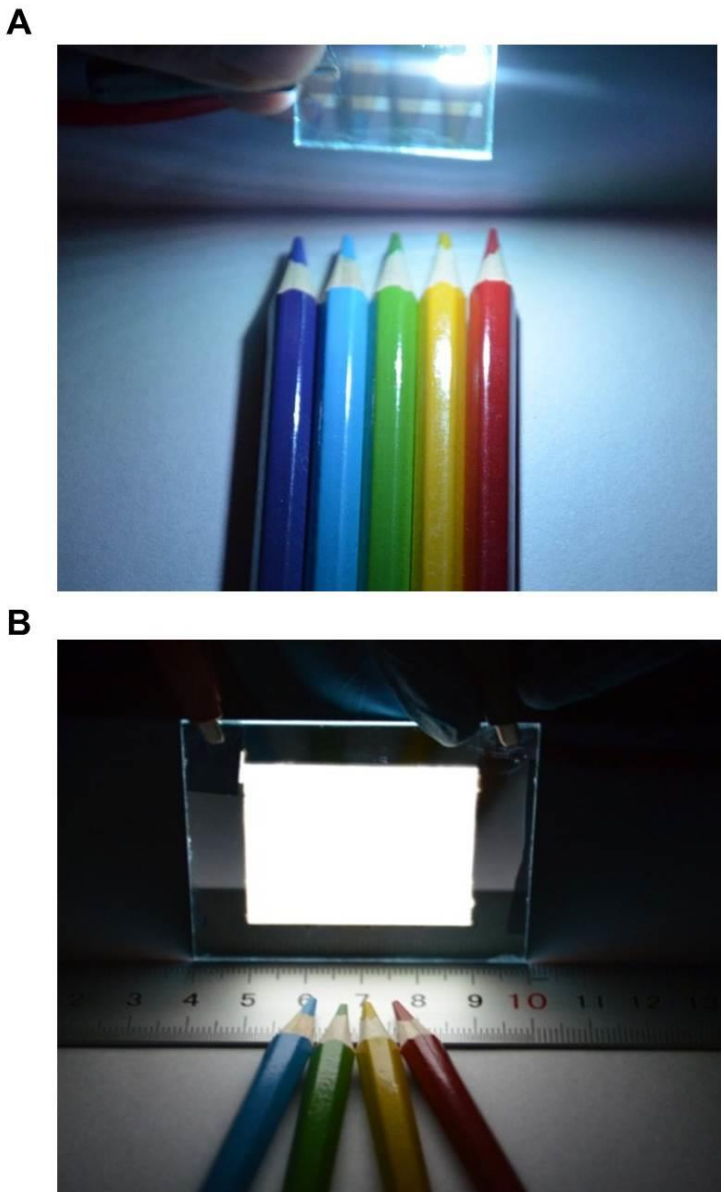

Figure S14. Photograph and demonstration of large-area white panel for the FIr-*p*-OC_8 based white device with a 0.4 wt. % content of Ir(FIpy-CF_3)$_3$. (**A**) Photograph for the white device, and (**B**) Demonstration of large-area white panel (40 mm × 40 mm) with the same configuration as the white device. Related to Figure 4.

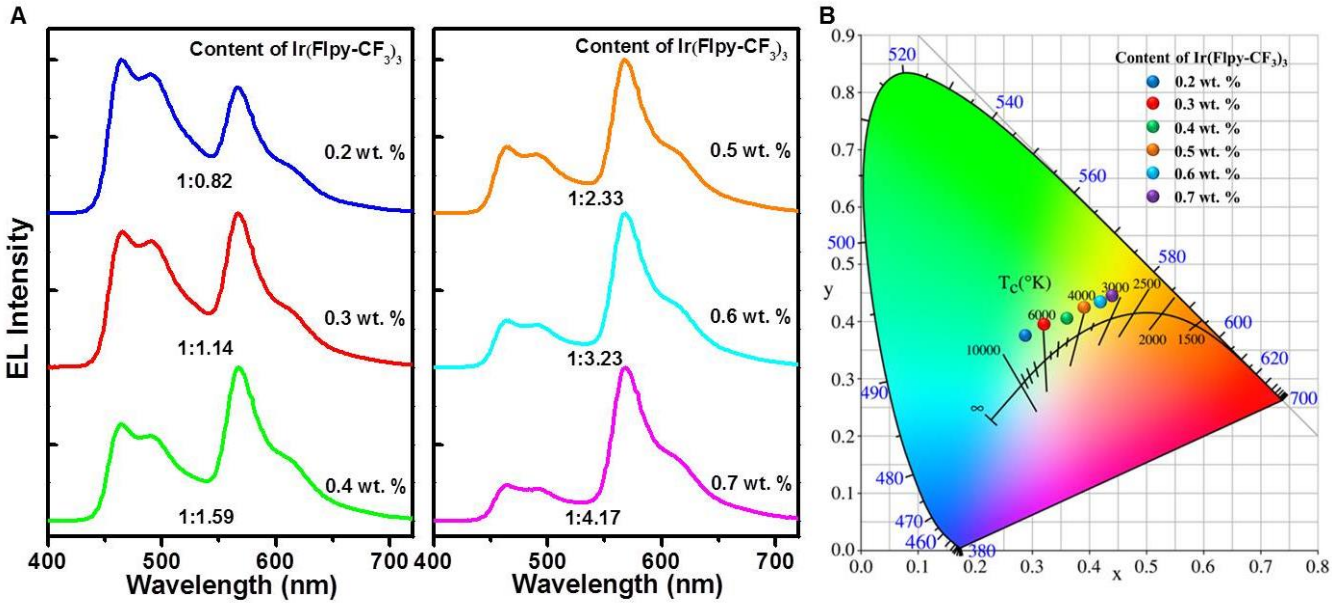

Figure S15. Tuning of CCT and CIE coordinates. (**A**) EL spectra of white devices with different content of Ir(Flpy-CF_3)$_3$. (**B**) CIE chromaticity diagram, where the corresponding CCT is also marked out. Related to Figure 4.

Tunable correlated color temperature (CCT) and CIE coordinates. Nearby the white point or equal energy point, the CCT should lie between 3000 and 10000 K to be suitable for different illumination requirements. For example, cool white light with high CCT will make humans feel refreshing, which is suitable for tropical zones or offices. But warm white light with low CCT will make humans feel warming and relaxing, which is suitable for frigid zones or night rest areas. With this idea in mind, the content of yellow phosphor Ir(Flpy-CF_3)$_3$ is changed to tune the CCT and CIE coordinates for the white device with out-coupling. By reducing the content from 0.4 wt. % to 0.3 and 0.2 wt. %, yellow emission intensity relative to blue emission in the EL spectra turns out to be smaller from 1.59 to 1.14 and 0.82 (Fig. S15A), leading to that the white light becomes cooler and cooler. The CCT correspondingly goes up from 4759 K to 5987 and 8113 K (Fig. S15B), and CIE coordinates shift from (0.36, 0.40) to (0.32, 0.39) and (0.29, 0.37). On the contrary, by increasing the content to 0.5, 0.6 and 0.7 wt. %, yellow emission intensity relative to blue emission in the EL spectra becomes lager to 2.33, 3.23 and 4.17, and the warm white light is obtained. The CCT correspondingly goes down to 3968, 3509 and 3240 K, and CIE coordinates shift to (0.39, 0.42), (0.42, 0.44) and (0.44, 0.44). More importantly, during the modulation of CCT, the power efficiency at 1000 cd m^{-2} maintains a relatively high level from 69.6 to 96.2 lm W^{-1} (corresponding to 33.0 to 47.0 lm W^{-1} for white device without out-coupling, Table S4), which is very important for its practical application in different illumination situations.

Supplemental Tables

Table S1. Summary of electrochemical properties for host and electron transporting materials. Related to Table 1 and Figure 3.

Material	E_{ox}[a] (V)	E_{red}[a] (V)	HOMO[b] (eV)	LUMO (eV)	T_1 (eV)
H2	0.48	--	-5.28	-1.91[c]	2.86[d]
TPCz	1.18	-2.54	-5.98	-2.26[b]	3.07 (Ding et al., 2010)
TmPyPB	1.41	-2.68	-6.21	-2.12[b]	2.78 (Su et al., 2008)

[a]E_{ox} is the first oxidation onset measured in DCM and E_{red} is the first reduction onset measured in DMF; [b]The HOMO and LUMO energy levels are calculated according to the equations: HOMO = -e(E_{ox} + 4.8V) and LUMO = -e(E_{red} + 4.8V); [c]The LUMO levels are calculated according to the equation: LUMO = HOMO + E_g, where E_g is the optical bandgap estimated from the absorption onset. [d]The triplet energy levels were calculated according to the phosphorescence peak wavelength positioned on the shortest wavelength side.

Table S2. Summary of blue device performance based on FIrpic and FIr-*p*-OC_8 with different doping concentration. Related to Figure 2**.**

Concentration (wt. %)	V_{on} (V)	Max performance			Device performance at 100/1000 cd m^{-2}				
		LE (cd A^{-1})	PE (lm W^{-1})	EQE (%)	V_d (V)	LE (cd A^{-1})	PE (lm W^{-1})	EQE (%)	CIE (x, y)
FIrpic									
1	3.9	14.8	10.5	7.4	4.7/5.6	14.3/10.2	9.7/5.7	7.1/5.1	(0.16, 0.30)
5	4.3	32.2	18.5	14.6	5.4/6.1	31.9/31.4	18.5/16.4	14.1/14.1	(0.15, 0.35)
15	4.5	32.6	17.8	14.4	5.6/6.3	31.1/32.2	17.8/16.0	14.0/14.2	(0.15, 0.36)
FIr-*p*-OC_8									
1	3.3	15.7	13.3	8.7	4.1/4.8	14.8/10.3	11.5/6.7	8.1/5.7	(0.16, 0.25)
5	3.1	30.3	26.7	15.7	4.0/4.5	29.9/24.8	23.9/17.4	15.5/12.9	(0.15, 0.26)
15	3.1	33.7	32.2	17.1	4.0/4.5	33.5/29.3	26.2/20.3	17.0/14.9	(0.15, 0.27)

Table S3. Summary of blue device performance based on FIr-*p*-OC_8 with high doping concentration. Related to Figure 4.

Concentration (wt.%)	V_{on} (V)	Max performance			Device performance at 100/ 1000 cd m^{-2}				
		LE (cd A^{-1})	PE (lm W^{-1})	EQE (%)	V_d (V)	LE (cd A^{-1})	PE (lm W^{-1})	EQE (%)	CIE (x, y)
20	2.9	34.3	33.3	18.2	3.7/4.3	34.2/30.2	28.6/22.1	18.1/16.0	(0.15, 0.26)
25	2.9	37.8	34.2	19.6	3.6/4.1	37.8/34.9	33.3/26.9	19.5/18.1	(0.15, 0.26)
30	2.9	33.6	33.6	17.5	3.5/4.2	33.5/30.5	30.1/22.8	17.4/15.9	(0.15, 0.26)

Table S4. Detail summary of the white device performance based on H2: 25 wt.% FIr-*p*-OC_8: x wt.% Ir(FIpy-CF_3)$_3$. Related to Figure 4 and Table 2.

White Device	V_{on} (V)	Max performance			Device performance at 1000/ 5000 cd m^{-2}				
		LE (cd A^{-1})	PE (lm W^{-1})	EQE (%)	V_d (V)	LE (cd A^{-1})	PE (lm W^{-1})	EQE (%)	CIE (x, y) at 1000 cd m^{-2}
x = 0.2 wt.%	3.0	52.9	47.6	20.4	4.3/4.9	44.1/27.5	33.0/18.0	17.8/11.5	(0.28, 0.36)
x = 0.2 wt.% (out-coupling)	2.9	104.9	98.2	40.3	4.1/4.5	89.1/67.1	69.6/47.1	35.7/27.6	(0.29, 0.37)
x = 0.3 wt.%	2.9	55.9	53.9	20.8	4.2/4.8	47.3/29.6	35.8/19.1	18.2/11.8	(0.31,0.38)
x = 0.3 wt.% (out-coupling)	2.8	114.1	110.7	42.0	4.0/4.4	102.4/78.7	81.7/56.8	38.9/31.0	(0.32, 0.39)
x = 0.4 wt.%	2.9	60.4	59.4	21.8	4.1/4.6	52.7/37.7	40.2/25.8	19.6/14.5	(0.34, 0.39)
x = 0.4 wt.% (out-coupling)	2.8	120.3	117.5	42.8	3.9/4.3	110.5/85.0	88.7/61.9	41.0/32.2	(0.36, 0.40)
x = 0.5 wt.%	2.8	65.6	67.7	22.9	4.4/4.8	55.1/38.5	42.2/26.4	19.8/14.3	(0.38, 0.41)
x = 0.5 wt.% (out-coupling)	2.8	116.3	109.6	40.3	4.0/4.4	107.3/84.1	84.8/60.7	38.1/31.0	(0.39, 0.42)
x = 0.6 wt.%	2.8	66.4	66.8	22.7	4.1/4.6	56.5/39.3	43.4/27.4	19.7/14.1	(0.41, 0.43)
x = 0.6 wt.% (out-coupling)	2.8	128.4	124.2	43.8	4.0/4.4	113.9/89.1	90.6/64.4	39.6/31.5	(0.42, 0.43)
x = 0.7 wt.%	2.8	69.1	68.5	23.6	4.1/4.6	59.7/43.1	47.0/29.8	20.6/15.4	(0.43, 0.44)
x = 0.7 wt.% (out-coupling)	2.8	131.5	130.1	44.6	3.9/4.3	119.5/95.0	96.3/69.0	40.9/33.0	(0.44, 0.44)

Transparent Methods

Materials. TmPyPB (1,3,5-tri(m-pyrid-3-yl-phenyl)benzene) and FIrpic were obtained from Luminescence Technology Corp. H2, $Ir(Flpy\text{-}CF_3)_3$ and TPCz (3,6-bis(diphenylphosphoryl)-9-(4'-(diphenylphosphoryl)phenyl)-carbazole) were prepared according to our previously reported methods (Zhang et al., 2012; Ding et al., 2009; Ding et al., 2010). The high-energy-level blue phosphors FIr-*m*-OC_8 and FIr-*p*-OC_8 were synthesized as described in the Supplemental Information.

Measurements and characterization. 1H and 19F nuclear magnetic resonance (NMR) spectra were obtained using Bruker Avance 400 NMR spectrometer. Elemental analysis was performed using an elemental analyzer from Bio-Rad Corporation. Mass spectra were measured using AXIMA-CFR, MALDI/TOF (matrix assisted laser desorption ionization/time-of-flight) spectrometer. UV-Vis absorption spectra were recorded using Perkin-Elmer Lambda 35 UV-Vis spectrometer. Photoluminescence (PL) spectra were measured with a Perkin-Elmer LS 50B spectrometer. Under an argon atmosphere, the PL decay characteristics were measured on LKS80 Laser Flash Photolysis Spectrometer (Applied Photophysics) in the PL transient measurement mode. The laser source is a tunable Nd: YAG-laser system (NT341a) with an excitaton wavelength of 355 nm (pulse duration: 4-6 ns, pulse repetition rate: 10 Hz). Lifetimes were obtained from the PL decay curves using a monoexponential fitting model. PLQYs in toluene solutions were measured using a spectrofluorimeter (Fluorolog-3, Horiba) equipped with a calibrated integrating sphere. The integrating sphere was purged with N_2 during measurements. The PLQYs were calculated by comparing the spectral intensities of the absorbed excitation light and the PL emission of the samples. Cyclic voltammetry (CV) experiments were performed on an EG&G 283 potentiostat/galvanostat system from Princeton Applied Research Corporation. Oxidation potential was tested in dichloromethane (DCM) and reduction potential was tested in dimethylformamide (DMF) at a scanning rate of 100 mV s^{-1}. A 0.1 M tetrabutylammonium perchlorate ($n\text{-}Bu_4NClO_4$) was used as the supporting electrolyte. By using ferrocene/ferrocenium couple as the reference (4.8 eV relative to the vacuum level), the HOMO and LUMO energy levels were calculated according to the two equations: $E_{HOMO} = -e(E_{ox} + 4.8\ V)$ and $E_{LUMO} = -e(E_{red} + 4.8\ V)$. An exception is the dendritic host H2, whose LUMO level is calculated according to the equation $E_{LUMO} = E_{HOMO} + E_g$. Here, E_{ox} and E_{red} were taken from the onset of the oxidation and reduction potential, respectively; E_g was the optical band gap estimated from the onset of the absorption spectrum. Thermal gravimetric analysis (TGA) and differential scanning calorimetry (DSC) were performed under a flow of nitrogen with Perkin-Elmer-TGA 7 and Perkin-Elmer-DSC 7 system, respectively.

Device fabrication and testing. Devices were fabricated with a configuration of ITO/PEDOT:PSS (40 nm)/EML (30 nm) /TPCz (8 nm)/TmPyPB (42 nm)/LiF (1 nm)/Al (100 nm). Hole-only devices were fabricated with a configuration of ITO/PEDOT:PSS (40 nm)/EML (85 nm) /MoO3 (5 nm)/Al (100 nm). The ITO substrates were firstly cleaned and UV-ozone treated for about 25 minutes. Then a 40 nm PEDOT:PSS (Clevios P Al 4083) was spin-coated onto the ITO surface. After being baked at 120 ℃ for 30 minutes in air condition, the substrates were transferred into a nitrogen-filled glovebox. Subsequently, a 30 nm (85 nm for hole-only devices) EML was spin-coated from chlorobenzene solution and annealed at 100 ℃ for 30 minutes. Finally, the upper layers of 8 nm

TPCz, 42 nm TmPyPB, 1 nm LiF and 100 nm Al (5 nm MoO_3 and 100 nm Al for hole-only devices) were evaporated in sequence via a shadow mask to finish the device fabrication in a vacuum chamber at a base pressure less than 4×10^{-4} Pa. The current density-voltage-luminance characteristics of the devices were measured using a Keithley source measurement unit (Keithley 2400 and Keithley 2000) equipped with a calibrated silicon photodiode. The EL spectra were recorded with CS2000 spectroscan photometer. The external quantum efficiency (EQE) was calculated based on the current density, luminance and EL spectral data. For the transient EL measurements, the devices were electrically excited by a pulse generator (Agilent 8114A, 100V/2A). Then the transient EL signals passed through a monochromator and were collected by a photomultiplier tube (PMT). The results were displayed on an oscilloscope (Agilent Model 54825A, 500 MHz/2 GSa/s).

DFT calculations. The Gaussian 09 was used to get the optimized structures and the corresponding energy values at B3LYP/genecp (6-31G* for C H O N F, Lanl2DZ for Ir) level (Frisch et al., 2009; Becke, 1993; Stephens et al., 1994; Lu and Chen, 2012), the minima was confirmed with all real frequencies. Based on Gaussian output files, the frontier molecular orbital and the triplet spin density distributions were obtained with Multiwfn. Firstly, the optimized structure of ground state (S_0) was obtained, and the total energy was denoted as $E(S_0)$. Then, with the formal check file, the HOMO and LUMO values were read and their distributions were visualized using Multiwfn (main function 0). After that, the optimized structure of the first triplet state (T_1) was obtained, and the total energy is denoted as $E(T_1)$. Finally, the triplet spin density distribution using Multiwfn (main function 5) was obtained, and the adiabatic energy of first triplet is calculated by $E(T_1) - E(S_0)$.

Supplemental References

Wang, Y., Wang, S., Shao, S., Ding, J., Wang, L., Jing, X., and Wang, F. (2015). Synthesis and properties of greenish-blue-emitting iridium dendrimers with N-phenylcarbazole-based polyether dendrons by a post-dendronization route. Dalton T. *44*, 1052-1059.

Wang, Y., Lu, Y., Gao, B., Wang, S., Ding, J., Wang, L., Jing, X., and Wang, F. (2015). Single molecular tuning of the charge balance in blue-emitting iridium dendrimers for efficient nondoped solution-processed phosphorescent OLEDs. Chem. Commun. *52*, 11508-11511.

Ding, J., Wang, Q., Zhao, L., Ma, D., Wang, L., Jing, X., and Wang, F. (2010). Design of star-shaped molecular architectures based on carbazole and phosphine oxide moieties: towards amorphous bipolar hosts with high triplet energy for efficient blue electrophosphorescent devices. J. Mater. Chem. *20*, 8126-8133.

Su, S.-J., Chiba, T., Takeda, T., and Kido, J. (2008). Pyridine-containing triphenylbenzene derivatives with high electron mobility for highly efficient phosphorescent OLEDs. Adv. Mater. *24*, 1873-1877.

Zhang, B., Tan, G., Lam, C.-S., Yao, B., Ho, C.-L., Liu, L., Xie, Z., Wong, W.-Y., Ding, J., and Wang, L. (2012). High-efficiency single emissive layer white organic light-emitting diodes based on solution-processed dendritic host and new orange-emitting iridium complex. Adv. Mater. *24*, 1873-1877.

Ding, J., Zhang, B., Lu, J., Xie, Z., Wang, L., Jing, X., and Wang, F. (2009). Solution-processable carbazole-based conjugated dendritic hosts for power-efficient blue-electrophosphorescent devices. Adv. Mater. *21*, 4983-4986.

Ding, J., Wang, Q., Zhao, L., Ma, D., Wang, L., Jing, X., and Wang, F. (2010). Design of star-shaped molecular architectures based on carbazole and phosphine oxide moieties: towards amorphous bipolar hosts with high triplet energy for efficient blue electrophosphorescent devices. J. Mater. Chem. *20*, 8126-8133.

Frisch, M. J., Trucks, G. W., Schlegel H. B. et al. Gaussian, Inc., Wallingford CT, 2009.

Becke, A. D. (1993). Density-functional thermochemistry. III. The role of exact exchange. J. Chem. Phys. *98*, 5648-5652.

Stephens, P. J., Devlin, F. J., Chabalowski, C. F., and Frisch, M. J. J. (1994). AB-INITIO CALCULATION OF VIBRATIONAL ABSORPTION AND CIRCULAR-DICHROISM SPECTRA USING DENSITY-FUNCTIONAL FORCE-FIELDS. J. Phys. Chem. *98*, 11623-11627.

Lu, T., and Chen, F. (2012). Multiwfn: A multifunctional wavefunction analyzer. J. Comput. Chem. *33*, 580-592.